

## ARTICLE OPEN



# Exploitation of ATP-sensitive potassium ion ( $K_{ATP}$ ) channels by HPV promotes cervical cancer cell proliferation by contributing to MAPK/AP-1 signalling

James A. Scarth<sup>1,2,4</sup>, Christopher W. Wasson<sup>1,2,5</sup>, Molly R. Patterson<sup>1,2</sup>, Debra Evans<sup>3</sup>, Diego Barba-Moreno<sup>1,2</sup>, Holli Carden<sup>1,2</sup>, Rosa Cassidy<sup>1,2</sup>, Adrian Whitehouse<sup>1,2</sup>, Jamel Mankouri<sup>1,2</sup>, Adel Samson<sup>3</sup>, Ethan L. Morgan<sup>1,2,6</sup>✉ and Andrew Macdonald<sup>1,2</sup>

© The Author(s) 2023

Persistent infection with high-risk human papillomaviruses (HPVs) is the causal factor in multiple human malignancies, including >99% of cervical cancers and a growing proportion of oropharyngeal cancers. Prolonged expression of the viral oncoproteins E6 and E7 is necessary for transformation to occur. Although some of the mechanisms by which these oncoproteins contribute to carcinogenesis are well-characterised, a comprehensive understanding of the signalling pathways manipulated by HPV is lacking. Here, we present the first evidence to our knowledge that the targeting of a host ion channel by HPV can contribute to cervical carcinogenesis. Through the use of pharmacological activators and inhibitors of ATP-sensitive potassium ion ( $K_{ATP}$ ) channels, we demonstrate that these channels are active in HPV-positive cells and that this activity is required for HPV oncoprotein expression. Further, expression of SUR1, which forms the regulatory subunit of the multimeric channel complex, was found to be upregulated in both HPV+ cervical cancer cells and in samples from patients with cervical disease, in a manner dependent on the E7 oncoprotein. Importantly, knockdown of SUR1 expression or  $K_{ATP}$  channel inhibition significantly impeded cell proliferation via induction of a G1 cell cycle phase arrest. This was confirmed both in vitro and in vivo tumourigenicity assays. Mechanistically, we propose that the pro-proliferative effect of  $K_{ATP}$  channels is mediated via the activation of a MAPK/AP-1 signalling axis. A complete characterisation of the role of  $K_{ATP}$  channels in HPV-associated cancer is now warranted in order to determine whether the licensed and clinically available inhibitors of these channels could constitute a potential novel therapy in the treatment of HPV-driven cervical cancer.

*Oncogene*; <https://doi.org/10.1038/s41388-023-02772-w>

## INTRODUCTION

It has been estimated that high-risk human papillomaviruses (HPVs) are the causal factor in over 5% of all human cancers, including >99.7% of cervical cancers and a growing number of oropharyngeal cancers [1, 2]. HPV16 is responsible for the majority of these (around 55% of cervical cancers and almost all HPV-positive (HPV+) head and neck cancers), whilst HPV18 is the cause of another 15% of cervical cancers [3]. As a result of this, cervical cancer is the fourth most prevalent cancer in women and the most common cause of cancer-related death in young women [1].

HPV-associated malignancies are the result of a persistent infection where the host immune system fails to detect and clear the virus efficiently, although even in this situation carcinogenesis may take several years to occur [1]. The most important factor required for initiation and progression of cancer is the prolonged increased expression of the viral oncoproteins E6 and E7, which results in the dysregulation of cell proliferation [4]. Some of the mechanisms by which the oncoproteins achieve this have been

widely-studied, including the ability of HPV E7 to drive S phase re-entry via binding to and inducing the degradation of pRb and the related pocket proteins p107 and p130 [5–7]. Concurrently, E6 targets p53 for proteasomal degradation by recruiting the E3 ubiquitin ligase E6-associated protein (E6AP) in order to block pro-apoptotic signalling [8]. Further, high-risk E6 proteins are also able to increase telomerase activity and bind to and regulate PSD95/DLG/ZO-1 (PDZ) domain-containing proteins in order to increase cell proliferation and survival [9, 10], whilst E7 has a key role in mediating evasion of the host immune response [11, 12]. More recently, E6 has been shown to modulate a multitude of host signalling pathways, including the JAK-STAT and Hippo pathways, during transformation [13–18].

However, a comprehensive understanding of the host signalling networks modulated by HPV during transformation is still lacking. Furthermore, no therapeutic targeting of viral proteins in HPV-driven malignancies currently exists. Therefore, it is necessary to identify novel HPV-host interactions and to establish whether they

<sup>1</sup>School of Molecular and Cellular Biology, Faculty of Biological Sciences, University of Leeds, Leeds LS2 9JT, UK. <sup>2</sup>Astbury Centre for Structural Molecular Biology, University of Leeds, Leeds LS2 9JT, UK. <sup>3</sup>Leeds Institute of Medical Research, St James's University Hospital, University of Leeds, Leeds LS9 7TF, UK. <sup>4</sup>Present address: Barts Cancer Institute, Queen Mary University of London, London EC1M 6BQ, UK. <sup>5</sup>Present address: Leeds Institute of Rheumatic and Musculoskeletal Medicine, Faculty of Medicine and Health, University of Leeds, Leeds LS2 9JT, UK. <sup>6</sup>Present address: School of Life Sciences, University of Sussex, Brighton BN1 9QG, UK. ✉email: em715@sussex.ac.uk; a.macdonald@leeds.ac.uk

Received: 14 February 2023 Revised: 13 June 2023 Accepted: 28 June 2023

Published online: 13 July 2023

may constitute potential new therapeutic targets. In particular, despite the availability of prophylactic vaccines, there are currently no effective anti-viral drugs for use against HPV. Current therapeutics rely on the widely-used yet non-specific DNA-damaging agent cisplatin in combination with radiotherapy [19, 20]. However, resistance to cisplatin, either intrinsic or acquired, is a significant problem [21]. Although this issue can be somewhat alleviated through the use of combination therapy involving cisplatin alongside paclitaxel, there is an urgent need to develop more targeted therapies for the treatment of HPV-associated malignancies [22].

Ion channels may represent ideal candidates for these novel therapies given the abundance of licensed and clinically available drugs targeting the complexes which could be repurposed if demonstrated to be effective [23]. Indeed, the importance of ion channels in the regulation of the cell cycle and cell proliferation has become increasingly recognised [24–28]. Cells undergo a rapid hyperpolarisation during progression through the G1-S phase checkpoint, which is then reversed during G2 [26]. It is thought that potassium ion ( $K^+$ ) channels are particularly important for this, with a number of  $K^+$  efflux channels having been observed to be increased in expression and activity during G1 [25, 26]. Of these, ATP-sensitive  $K^+$  ( $K_{ATP}$ ) channels have been shown to be expressed highly in some cancers, and channel inhibition can result in decreased proliferation [29–33].

$K_{ATP}$  channels are hetero-octameric membrane complexes consisting of four pore-forming Kir6.x subunits (either Kir6.1 or Kir6.2) surrounded by four regulatory sulfonylurea receptor (SUR) subunits [34]. Multiple isoforms of the sulfonylurea receptor exist: SUR1 (encoded by *ABCC8*); and SUR2A and SUR2B, which are produced via alternative splicing of the *ABCC9* transcript [35].  $K_{ATP}$  channels are expressed in multiple tissues, although the composition of the channels can vary, which may account for subtle tissue-specific properties of the channels [34].  $K_{ATP}$  channels are involved in the control of insulin secretion from pancreatic beta cells in response to alterations to the blood glucose concentration, but are also critical in protecting cardiac tissue from ischaemia-induced injury and play a role in the regulation of blood pressure by smooth muscle cells of the vasculature [36].

In this study, we performed a pharmacological screen to identify  $K^+$  channels that may play a role in HPV pathogenesis. We identified that, of the  $K^+$  channels investigated, inhibition of  $K_{ATP}$  channels had a negative impact on HPV oncoprotein expression and cellular transformation. By screening for the expression of  $K_{ATP}$  channel subunits, we identified that the SUR1 subunit is expressed highly in HPV+ cervical cancer cells, and that this increased SUR1 expression is driven by the E7 oncoprotein. Depletion of  $K_{ATP}$  channel activity, either by siRNA-mediated knockdown or pharmacological inhibition, significantly impeded proliferation and cell cycle progression. Further, we propose that this pro-proliferative effect is mediated via the activation of a mitogen-activated protein kinase (MAPK)/activator protein-1 (AP-1) signalling axis. We hope that the targeting of  $K_{ATP}$  channels may prove to be beneficial in the treatment of HPV-associated cervical neoplasia.

## RESULTS

### $K_{ATP}$ channels are important for HPV gene expression in cervical cancer cells and primary human keratinocytes

Ion channels are emerging as crucial regulators of cell signalling pathways and cell cycle progression [24–27]. In particular,  $K^+$  channels have been shown to be active or expressed highly in a variety of cancer cell lines [37, 38]. Furthermore, a growing number of viruses have been shown to be capable of modulating the activity of host ion channels [39]. To determine whether HPV requires the activity of  $K^+$  channels either during its life cycle or during transformation, we performed a pharmacological screen

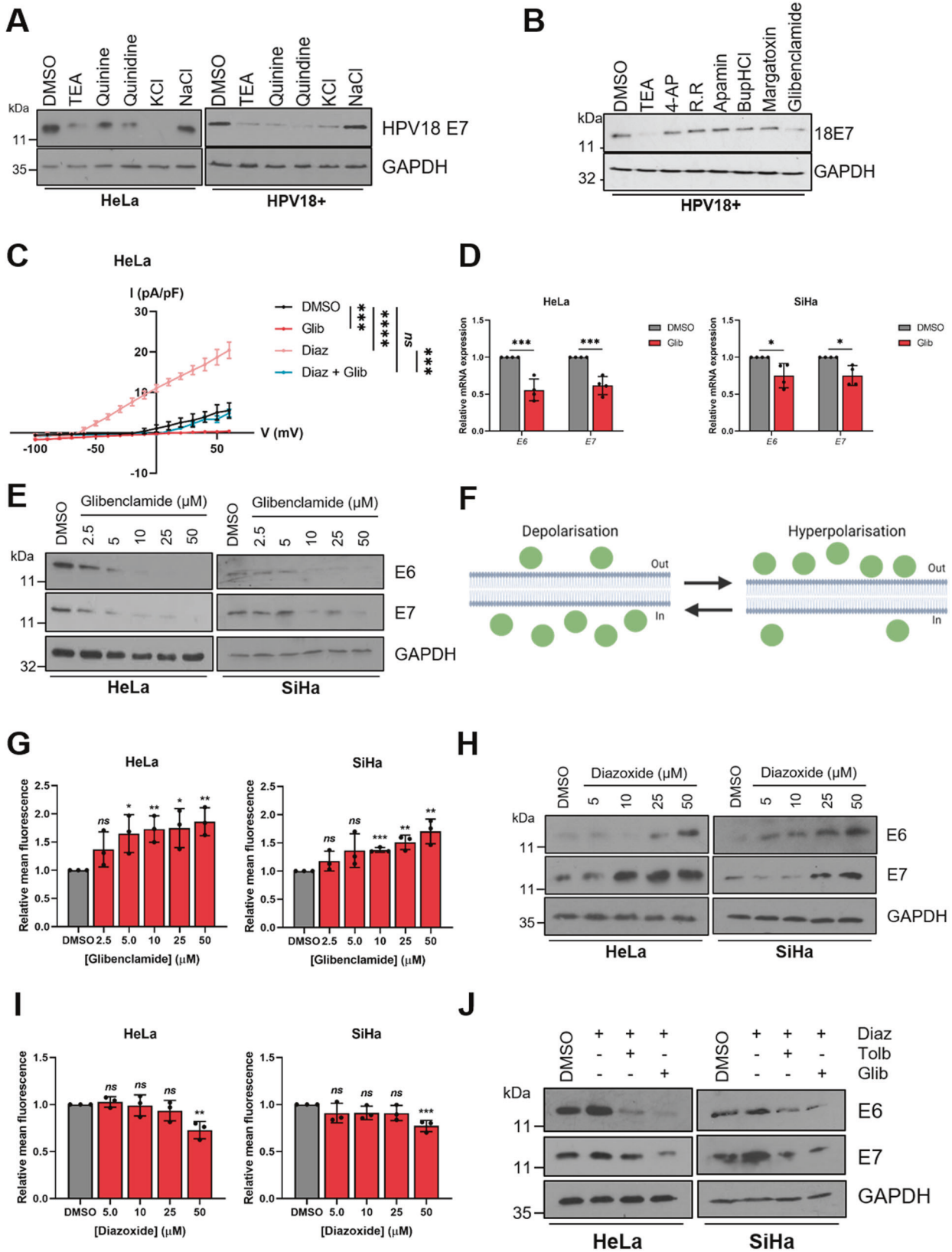
using several broadly-acting  $K^+$  channel modulators. We first assessed the impact of  $K^+$  channel inhibition on the expression of the viral oncoprotein E7, which is essential for the survival and proliferation of cervical cancer cells both in vitro and in vivo [40–42]. Treatment of either HPV18+ cervical cancer cells (HeLa) or primary human keratinocytes containing the HPV18 genome with tetraethylammonium (TEA), quinine or quinidine at pharmacologically relevant concentrations resulted in a decrease in E7 oncoprotein expression (Fig. 1A), indicating that HPV does indeed require the activity of  $K^+$  channels. Addition of potassium chloride (KCl) to increase the extracellular  $K^+$  concentration and thus collapse the plasma membrane potential had the same effect on oncoprotein expression, but addition of sodium chloride (NaCl) had no impact, indicating that alteration of osmolarity alone does not impact upon HPV gene expression (Fig. 1A).

In order to identify whether a particular class of  $K^+$  channels was required for HPV gene expression, a further screen was performed using more specific  $K^+$  channel inhibitors. Treatment with inhibitors of voltage-gated  $K^+$  channels (4-aminopyridine (4-AP) or margatoxin), two-pore-domain  $K^+$  channels (ruthenium red (RR) or bupivacaine hydrochloride (BupHCl)) or calcium-activated  $K^+$  channels (apamin) had no impact on E7 protein levels (Fig. 1B). However, treatment with glibenclamide, a clinically available inhibitor of  $K_{ATP}$  channels which acts via binding to the regulatory SUR subunits [43], resulted in a marked decrease in E7 expression in HPV18-containing primary keratinocytes (Fig. 1B).

Next, electrophysiological analysis was performed in HeLa cells to confirm that active  $K_{ATP}$  channels were present. A clear outward  $K^+$  current was observed, which was significantly increased upon application of the  $K_{ATP}$  channel activator diazoxide (Fig. 1C). This was entirely reversed after addition of the channel inhibitor glibenclamide, whilst glibenclamide treatment alone was able to reduce basal  $K^+$  currents. Together, this confirms that active  $K_{ATP}$  channels are present in cervical cancer cells.

To further investigate the repressive effects of glibenclamide on the HPV oncoproteins, expression levels were assayed after treatment of both HPV16+ and HPV18+ cervical cancer cells with the inhibitor at a range of concentrations. A significant decrease in expression of both E6 and E7 was observed at both the mRNA level (Fig. 1D) and the protein level (Fig. 1E) at concentrations as low as 10  $\mu$ M. To ensure that the effect of glibenclamide treatment on viral oncoprotein expression was due to the inhibition of  $K_{ATP}$  channel activity, we first analysed the membrane potential of cells using the fluorescent dye Bis-(1,3-Dibutylbarbituric Acid) Trimethine Oxonol (DiBAC<sub>4</sub>(3)) [44, 45]. The ability of the dye to enter cells is proportional to the degree to which the plasma membrane is depolarised (Fig. 1F). Therefore, the dose-dependent increase in fluorescence observed following glibenclamide treatment indicates an increasing level of depolarisation, consistent with a reduction in  $K_{ATP}$  channel opening (Fig. 1G). Significantly, treatment of cells with tolbutamide, a member of the same class of sulfonylurea drugs as glibenclamide, also resulted in a dose-dependent decrease in oncoprotein expression with a corresponding increase in DiBAC<sub>4</sub>(3) fluorescence (Fig. S1A–C).

In line with our inhibitor data, treatment of HPV+ cervical cancer cells with the  $K_{ATP}$  channel activator diazoxide resulted in a dose-dependent increase in HPV oncoprotein expression (Fig. 1H). As before, analysis of DiBAC<sub>4</sub>(3) fluorescence was performed to assess the impact of diazoxide treatment on the plasma membrane potential. A decrease in fluorescence, particularly apparent at the highest concentration of 50  $\mu$ M, was observed after application of diazoxide, indicating increasing levels of hyperpolarisation (Fig. 1I). Finally, treatment of HPV+ cervical cancer cells with either glibenclamide or tolbutamide abolished the diazoxide-induced increase in HPV oncoprotein expression (Fig. 1J). Taken together, these data demonstrate that  $K_{ATP}$  channel activity is important in the regulation of HPV gene expression.



**HPV upregulates the SUR1 subunit of K<sub>ATP</sub> channels**

Given the importance of K<sub>ATP</sub> channel activity for HPV oncoprotein expression, we hypothesised that HPV may upregulate expression of channel subunits. Notably, the expression of K<sub>ATP</sub> channel

subunits displays significant tissue-specific variability, so it was important to gain an understanding of which isoforms are expressed in cervical tissue [36]. We therefore screened for the expression of all K<sub>ATP</sub> channel subunits in a panel of cervical

**Fig. 1** **K<sub>ATP</sub> channels are important for HPV gene expression.** **A** Representative western blots for E7 expression in HeLa cells and primary human keratinocytes containing HPV18 episomes treated with DMSO, a broadly-acting K<sup>+</sup> channel inhibitor (25 mM tetraethylammonium (TEA), 100 μM quinine, 100 μM quinidine or 70 mM KCl) or 70 mM NaCl. GAPDH served as a loading control. **B** Representative western blots for E7 expression in HPV18<sup>+</sup> primary keratinocytes treated with DMSO, 25 mM TEA or one of a panel of class-specific K<sup>+</sup> channel inhibitors (2 mM 4-aminopyridine (4-AP), 50 μM ruthenium red (RR), 10 nM apamin, 20 μM bupivacaine hydrochloride (BupHCl), 10 nM margatoxin or 50 μM glibenclamide). GAPDH served as a loading control. **C** Mean current density-voltage relationships for K<sup>+</sup> currents in HeLa cells treated with DMSO, diazoxide (50 μM), glibenclamide (10 μM), or both diazoxide and glibenclamide (*n* = 5 for all treatments). **D** Expression levels of E6 and E7 mRNA in HeLa and SiHa cells treated with glibenclamide (10 μM) measured by RT-qPCR (*n* = 4 for all treatments). Samples were normalised against U6 mRNA levels. **E** Representative western blots of E6 and E7 expression in HeLa and SiHa cells treated with increasing doses of glibenclamide. GAPDH served as a loading control. **F** Schematic illustrating the plasma membrane permeability of DiBAC<sub>4</sub>(3). Figure created using BioRENDER.com. **G** Mean DiBAC<sub>4</sub>(3) fluorescence levels in HeLa and SiHa cells treated with increasing dose of glibenclamide. Samples were normalised to DMSO controls. **H** Representative western blots of E6 and E7 expression in HeLa and SiHa cells serum starved for 24 h (to reduce basal E6/E7 expression) prior to treatment with increasing doses of diazoxide. GAPDH served as a loading control. **I** Mean DiBAC<sub>4</sub>(3) fluorescence levels in HeLa and SiHa cells treated with increasing dose of diazoxide. Samples were normalised to DMSO control. **J** Representative western blots of E6 and E7 expression in HeLa and SiHa cells treated with diazoxide (50 μM) alone or in combination with glibenclamide (10 μM) or tolbutamide (200 μM). Bars represent means ± standard deviation (SD) of three biological replicates (unless stated otherwise) with individual data points displayed where possible. *Ns* not significant, \**P* < 0.05, \*\**P* < 0.01, \*\*\**P* < 0.001 (Student's *t* test).

cancer cell lines by RT-qPCR. K<sub>ATP</sub> channels are hetero-octameric complexes consisting of four pore-forming Kir6.x subunits (either Kir6.1 or Kir6.2) surrounded by four regulatory SURx subunits (either SUR1, SUR2A or SUR2B) [34]. We found no significant difference in the expression of Kir6.1 (*KCNJ8*), whilst Kir6.2 (*KCNJ11*) expression was higher in HPV-negative (HPV-) C33A cells, as well as three of the four HPV+ cervical cancer cell lines, when compared with normal human keratinocytes (NHKs) (Fig. 2A). Expression of SUR2A (*ABCC9A*) could not be detected in any of the cell lines, and SUR2B (*ABCC9B*) was not significantly increased in any of the HPV+ cell lines relative to NHKs. However, expression of the SUR1 (*ABCC8*) subunit was significantly higher in all four of the HPV+ cancer cell lines examined, with no increase detected in HPV- C33A cells. We attempted to confirm these findings by analysing K<sub>ATP</sub> channel subunit protein expression, but this was precluded by the dearth of high-quality, western blot-suitable antibody reagents specific to these cellular targets. Nevertheless, we elected to focus on the SUR1 subunit for the purposes of this study due to the consistent upregulation of expression we observed in the HPV+ cancer cell lines.

To further investigate the increased SUR1 expression potentially induced by HPV, we analysed cell lines containing episomal HPV18 generated from primary foreskin keratinocytes. The presence of HPV18 episomes in these cells has previously been validated [13, 46]. Transcript levels of *ABCC8* (SUR1) were significantly increased by approximately 10 fold relative to the NHK control (Fig. 2B). In addition, sections of organotypic raft cultures of NHKs and HPV18-containing keratinocytes, which recapitulate all stages of the HPV life cycle [47], were analysed for SUR1 protein levels by immunofluorescence microscopy. This demonstrated a marked increase in SUR1 protein expression in HPV18+ rafts in comparison to NHK raft cultures, consistent across both donors (Fig. 2C). Next, SUR1 expression was analysed in cervical liquid-based cytology samples from a cohort of HPV16+ patients representing the progression of cervical disease development (CIN 1 – CIN 3). We observed an increase in *ABCC8* (SUR1) mRNA levels relative to HPV- normal cervical tissue which correlated with disease progression, with the highest expression observed in CIN 3 samples (Fig. 2D). Indeed, immunofluorescence microscopy analysis of human cervical sections classified as LSIL (CIN 1), LSIL with foci of HSIL (CIN 1/2) and HSIL (CIN 3), confirmed that SUR1 protein levels increase with cervical disease progression (Fig. 2E).

Furthermore, SUR1 protein levels were analysed using the HPV16+ W12 in vitro model system [13, 48]. At low passage numbers, these cells display an LSIL phenotype in raft culture, but long-term passaging results in a phenotype more closely mirroring that of HSIL and squamous cell carcinoma. Raft cultures were generated from NHKs and a W12 clone representing a HSIL phenotype and stained for SUR1 protein levels. High levels of SUR1 staining were observed in the HSIL raft compared to the NHK

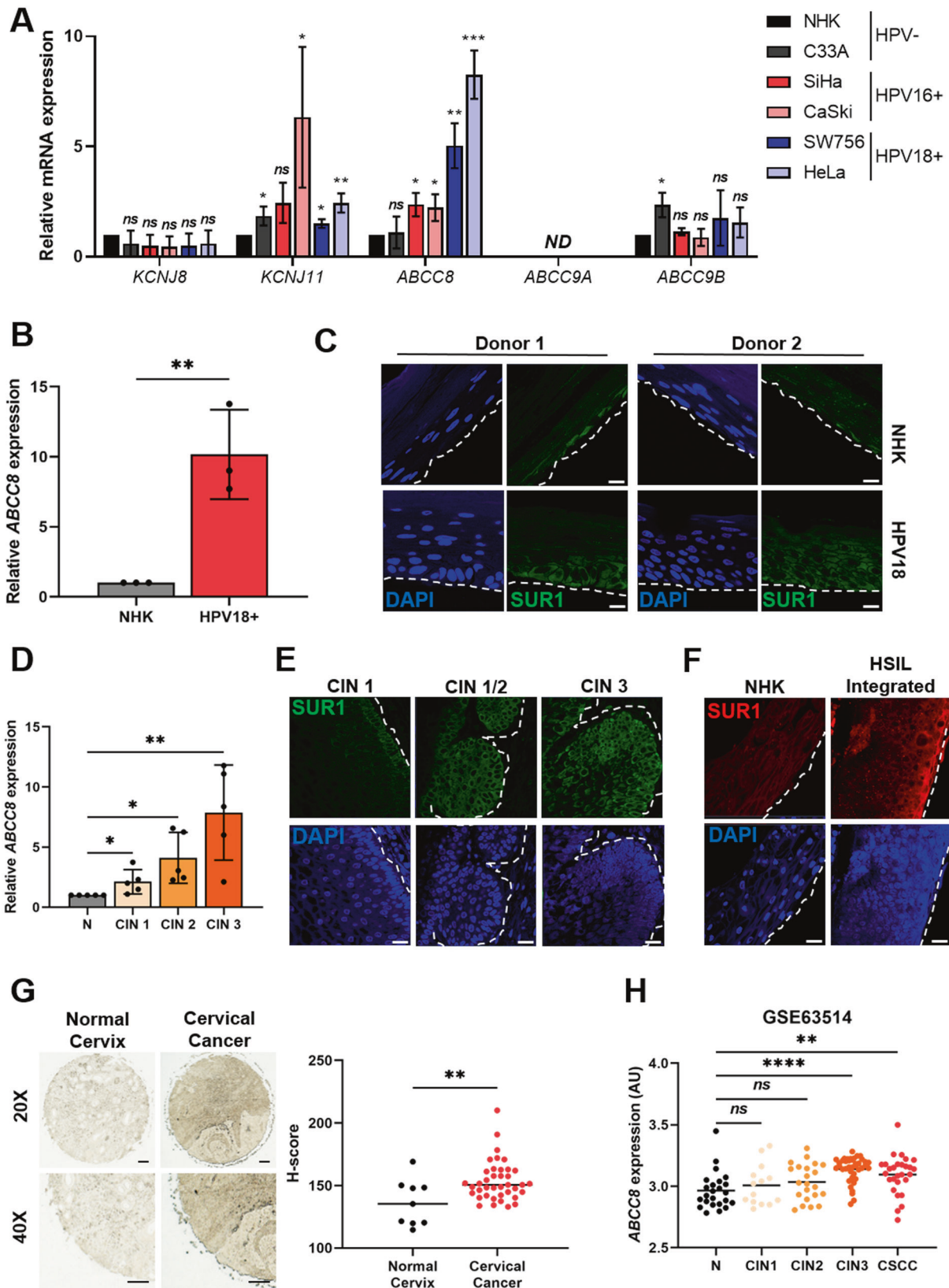
control (Fig. 2F), thus confirming that SUR1 expression increases with cervical disease progression. In order to analyse SUR1 protein levels in cervical cancer tissue, we performed immunohistochemistry using an array of normal cervix and cervical cancer tissue sections. Significantly higher SUR1 expression was observed in the cancer tissue sections, as indicated by an increase in H-score (Fig. 2G). Finally, to confirm our above observations, we mined an available microarray database containing data from primary cervical disease and tumour samples. This revealed a significant increase in *ABCC8* (SUR1) expression in the CIN 3 and cervical squamous cell carcinoma (CSCC) samples (Fig. 2H). Taken together, these data indicate that SUR1 expression is increased in HPV-containing keratinocytes and, importantly, in HPV-associated cervical disease.

#### Depletion of SUR1 reduces HPV gene expression in cervical cancer cells

After identifying that the SUR1 subunit of K<sub>ATP</sub> channels was highly expressed during HPV+ cervical disease, we investigated the effects of suppressing SUR1 expression. Knockdown of SUR1 using a pool of specific siRNAs was performed in both HPV16+ (SiHa) and HPV18+ (HeLa) cervical cancer cells (Fig. 3A). Furthermore, monoclonal HeLa cell lines stably expressing one of two SUR1-specific shRNAs were also generated (Fig. 3B). To ascertain the effect of SUR1 depletion on the plasma membrane potential, DiBAC<sub>4</sub>(3) fluorescence was used. We observed a ~2 fold increase in fluorescence after siRNA treatment, indicating a significant depolarisation characteristic of a reduction in K<sub>ATP</sub> channel activity (Fig. 3C). We were unable to analyse the impact of stable suppression of SUR1 on the plasma membrane potential due to the presence of a ZsGreen selectable marker.

Subsequently, the effect of SUR1 depletion on HPV gene expression was analysed. siRNA-mediated knockdown of SUR1 resulted in a significant decrease in HPV oncoprotein expression, measured both at the transcript and protein level (Fig. 3D, F). The same impact on HPV gene expression was also observed following stable knockdown of SUR1, when compared to cells expressing a non-targeting shRNA (shNTC) (Fig. 3E, G). To confirm that the effect of SUR1 depletion on HPV gene expression was due to a direct loss of transcription from the viral upstream regulatory region (URR), luciferase reporters containing the HPV16 and HPV18 URRs were used. We observed a significant decrease in relative luciferase activity after SUR1 knockdown with both URR reporter plasmids, confirming a direct loss of HPV early promoter activity (Fig. 3H).

In contrast to this, transfection of a pool of SUR2-specific siRNAs had no impact on HPV oncoprotein expression in either HPV16+ or HPV18+ cervical cancer cells, in line with our data showing that HPV does not induce an increase in expression of the SUR2 subunit of K<sub>ATP</sub> channels (Fig. S2A–D). We did however observe a small depolarisation of the plasma membrane, indicated by an



increase in DiBAC<sub>4</sub>(3) fluorescence (Fig. S2B), suggesting that a small minority of K<sub>ATP</sub> channels in HPV+ cervical cancer cells may be composed of the SUR2 subunit.

Finally, in order to confirm that the effects on HPV gene expression observed were K<sub>ATP</sub> channel-dependent, rather than a

potential channel-independent function of SUR1, Kir6.2 levels were also depleted using a pool of specific siRNAs (Fig. S3A). The ~ 2 fold and ~ 1.5 fold increases in DiBAC<sub>4</sub>(3) fluorescence resulting from Kir6.2 knockdown observed in HeLa and SiHa cells respectively were broadly in line with the changes observed

**Fig. 2 HPV enhances expression of the SUR1 subunit of  $K_{ATP}$  channels.** **A** mRNA expression levels of  $K_{ATP}$  channel subunits in HPV- normal human keratinocytes (NHK) and a panel of five cervical cancer cell lines – one HPV- (C33A), two HPV16+ (SiHa and CaSki), and two HPV18+ (SW756 and HeLa) detected by RT-qPCR. Samples were normalised against *U6* mRNA levels. Data are displayed relative to NHK controls. **B** *ABCC8* mRNA expression in NHKs and keratinocytes containing episomal HPV18 genomes detected by RT-qPCR. Samples were normalised against *U6* mRNA levels. **C** Representative immunofluorescence analysis of sections from organotypic raft cultures of NHK and HPV18+ keratinocytes detecting SUR1 levels. Nuclei were visualised with DAPI and the white dotted line indicates the basal layer. Two donor cell lines were used to exclude donor-specific effects. Images were acquired with identical exposure times. Scale bar, 40  $\mu$ m. **D** *ABCC8* mRNA expression in a panel of cervical cytology samples representing normal cervical tissue (N) and cervical disease of increasing severity (CIN 1 - 3) detected by RT-qPCR ( $n = 5$  from each grade). Samples were normalised against *U6* mRNA levels. **E** Representative immunofluorescence analysis of tissue sections from cervical lesions of increasing CIN grade. Sections were stained for SUR1 levels (green) and nuclei were visualised with DAPI (blue). Images were acquired with identical exposure times and the white dotted line indicates the basal layer. Scale bar, 40  $\mu$ m. **F** Representative immunofluorescence analysis of sections from organotypic raft cultures of NHK and a W12 cell line presenting with HSIL morphology detecting SUR1 levels (red). Nuclei were visualised with DAPI (blue) and the white dotted line indicates the basal layer. Images were acquired with identical exposure times. Scale bar, 40  $\mu$ m. **G** Representative immunohistochemistry analysis and scatter dot plots of quantification of normal cervical ( $n = 9$ ) and cervical cancer ( $n = 39$ ) tissue sections stained for SUR1 protein. Scale bar, 50  $\mu$ m. **H** Scatter dot plot of expression data acquired from the GSE63514 dataset. Arbitrary values for *ABCC8* mRNA expression in normal cervix ( $n = 24$ ), CIN1 lesions ( $n = 14$ ), CIN2 lesions ( $n = 22$ ), CIN3 lesions ( $n = 40$ ) and cervical cancer ( $n = 28$ ) samples were plotted. Bars represent means  $\pm$  SD of three biological replicates, unless stated otherwise, with individual data points displayed where possible. *Ns* not significant, \* $P < 0.05$ , \*\* $P < 0.01$ , \*\*\* $P < 0.001$ , \*\*\*\* $P < 0.0001$  (Student's *t* test).

following SUR1 knockdown (Fig. S3B). Knockdown of Kir6.2 resulted in a significant reduction in both mRNA and protein levels of E6 and E7 to a similar extent to that detected following SUR1 knockdown (Fig. S3C, D), thus confirming that the impacts of SUR1 depletion were indeed channel-dependent. Taken together, these data confirm that  $K_{ATP}$  channel expression in cervical cancer cells is important for HPV oncoprotein expression.

#### The E7 oncoprotein is responsible for the increased SUR1 expression in HPV+ cervical cancer cells

We next explored the mechanism behind the observed HPV-induced increases in SUR1 expression. Given that the E6 and E7 oncoproteins are key drivers of transformation, we hypothesised that they may be responsible for the heightened SUR1 levels [2]. To investigate this, expression of both the E6 and E7 oncoproteins was repressed using siRNA in HPV+ cervical cancer cell lines. We saw a > 70% decrease in *ABCC8* (SUR1) mRNA levels after knockdown of oncoprotein expression (Fig. 4A). A decrease in *ABCC8* mRNA expression could also be observed after silencing of E6 and E7 in HPV18+ primary keratinocytes (Fig. 4B), indicating that oncoprotein expression is necessary to induce SUR1 expression. In order to gain an understanding of which oncoprotein drives this, the E6 and E7 oncoproteins of HPV18 were overexpressed in turn and in combination in HPV- C33A cells. HPV18 E6 did not result in any change in *ABCC8* mRNA levels, whereas in contrast, expression of E7 led to a ~2.5 fold increase in *ABCC8* expression (Fig. 4C). Co-expression of E6 alongside E7 did not cause a further increase in *ABCC8* mRNA levels, indicating that the E7 oncoprotein is the major driver of SUR1 expression. Similar effects on *ABCC8* mRNA levels were observed when this was performed in NHKs (Fig. 4D). Further, C33A cell lines stably expressing HA-tagged HPV18 oncoproteins were generated as previously described [18]. A significant upregulation of *ABCC8* expression was only observed in the HA-E7 expressing cells, consistent with our transient over-expression data (Fig. 4E).

To confirm that the observed changes in SUR1 expression led to an impact on  $K_{ATP}$  channel activity, the plasma membrane potential of cells was assayed after overexpression of HPV18 E7 in HPV- cervical cancer cells. A significant reduction in DiBAC<sub>4</sub>(3) fluorescence, indicative of membrane hyperpolarisation, was detected (Fig. 4F, G). This decrease was abolished both by treatment with glibenclamide and by siRNA-mediated knockdown of SUR1, suggesting that the hyperpolarisation was due to an E7-dependent increase in  $K_{ATP}$  channel activity. In addition, silencing of HPV E7 expression resulted in a ~2 fold increase in DiBAC<sub>4</sub>(3) fluorescence (Fig. 4H), consistent with a reduction in  $K_{ATP}$  channel opening. These data indicate that the E7 oncoprotein, rather than

E6, is the major factor regulating HPV-induced increases in SUR1 expression.

#### $K_{ATP}$ channels drive proliferation in HPV+ cervical cancer cells

Given the effects of  $K_{ATP}$  channel activity on HPV gene expression, it was hypothesised that modulation of channel activity may too impact upon the proliferation of HPV+ cervical cancer cells. Treatment of both HPV16+ SiHa cells and HPV18+ HeLa cells with glibenclamide to inhibit  $K_{ATP}$  channel activity resulted in a significant decrease in cell proliferation (Fig. 5A), anchorage-dependent (Fig. 5B) and anchorage-independent colony formation (Fig. 5C). In contrast, treatment of HPV- C33A cells with glibenclamide had minimal impact on proliferation or colony-forming ability (Fig. 5A–C).

To eliminate the possibility of off-target effects of glibenclamide, a pool of SUR1-specific siRNAs was used to confirm the impact of reduced  $K_{ATP}$  channel activity on HPV+ cervical cancer cell proliferation. Both HPV16+ and HPV18+ cells demonstrated a reduced proliferation rate (Fig. 5D) and colony-forming ability (Fig. 5E, F) after depletion of SUR1 levels. Further, stable suppression of SUR1 levels via the expression of specific shRNAs resulted in a similar or greater impact on proliferation, and the anchorage-dependent and anchorage-independent colony-forming ability of HPV18+ cervical cancer cells (Fig. S4A–C). In contrast, depletion of the alternative  $K_{ATP}$  channel regulatory subunit SUR2 had a minimal impact on the proliferation and colony-forming ability of both HPV+ cervical cancer cell lines analysed (Fig. S2E–G). This is consistent with our data showing a lack of an effect on HPV oncoprotein expression after silencing of SUR2.

Finally, to confirm that the reduction in proliferation observed after either glibenclamide treatment or suppression of SUR1 expression was a result of decreased  $K_{ATP}$  channel activity, we analysed the growth of HPV+ cervical cancer cells following siRNA depletion of the pore-forming Kir6.2 subunit. This resulted in a decrease in proliferation and colony formation in both HPV16+ and HPV18+ cervical cancer cells, concordant with that observed following SUR1 depletion (Fig. S3E–G). Collectively, these data demonstrate that  $K_{ATP}$  channels are important drivers of proliferation in HPV+ cervical cancer cells.

#### $K_{ATP}$ channel overexpression is sufficient to stimulate proliferation in the absence of HPV

Given the emerging evidence indicating that  $K_{ATP}$  channel activation can promote proliferation, and that heightened channel expression has been demonstrated in some other cancer types [29–33], we hypothesised that overexpression of  $K_{ATP}$  channel subunits alone (i.e. in the absence of HPV) may be sufficient to increase proliferation of cervical cancer cells. The individual

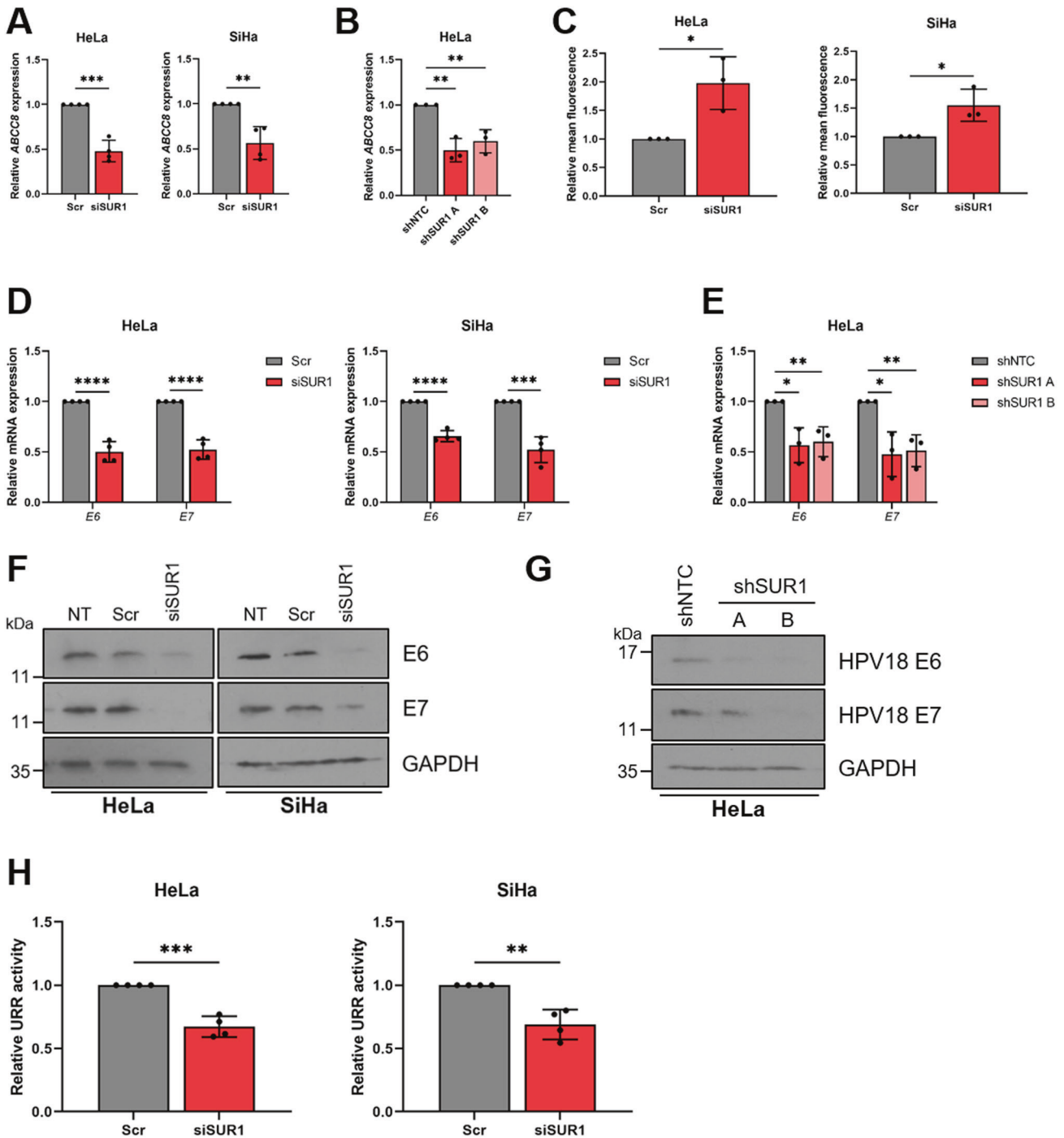
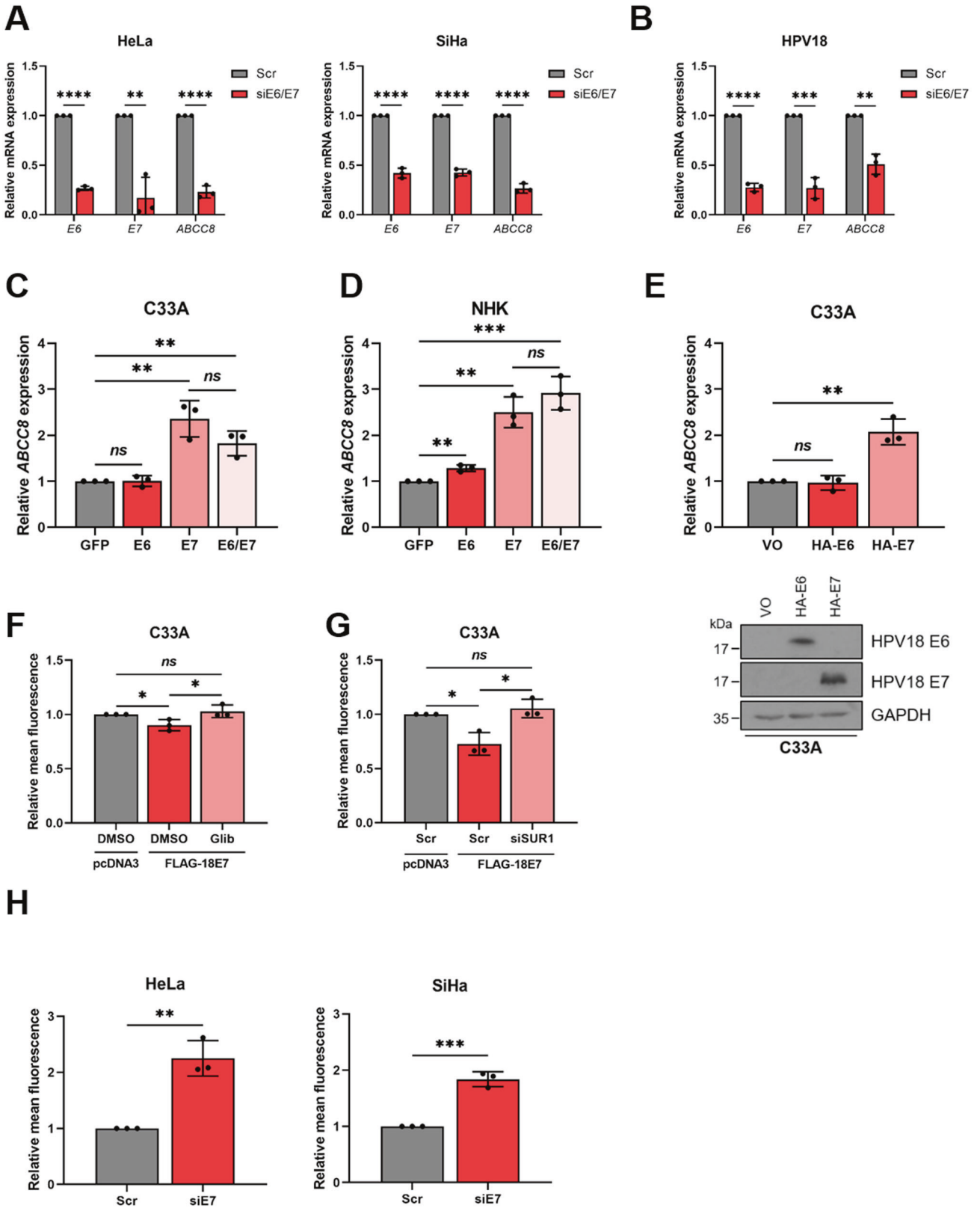


**Fig. 3** Depletion of SUR1 reduces HPV gene expression in cervical cancer cells. **A, B** Relative expression of *ABCC8* mRNA in **(A)** HeLa and SiHa cells transfected with a pool of SUR1-specific siRNA ( $n = 4$ ) and **(B)** two monoclonal HeLa cell lines stably expressing SUR1-specific shRNAs measured by RT-qPCR. Samples were normalised against *U6* mRNA levels. **C** Relative mean DiBAC<sub>4</sub>(3) fluorescence levels in HeLa and SiHa cells transfected with SUR1 siRNA ( $n = 4$ ) and **(E)** HeLa cell lines stably expressing SUR1-specific shRNAs measured by RT-qPCR. Samples were normalised against *U6* mRNA levels. **D, E** Relative expression of *E6* and *E7* mRNA in **(D)** HeLa and SiHa cells transfected with SUR1 siRNA ( $n = 4$ ) and **(E)** HeLa cell lines stably expressing SUR1-specific shRNAs measured by RT-qPCR. Samples were normalised against *U6* mRNA levels. **F, G** Representative western blots of *E6* and *E7* expression in **(F)** HeLa and SiHa cells transfected with SUR1 siRNA and **(G)** HeLa cell lines stably expressing either a non-targeting (shNTC) or a SUR1-specific shRNA. GAPDH served as a loading control. **H** Relative firefly luminescence in HeLa and SiHa cells co-transfected with SUR1 siRNA and either a HPV18 or HPV16 URR reporter plasmid respectively ( $n = 4$  for all conditions). Luminescence values were normalised against *Renilla* luciferase activity and data is displayed relative to scramble controls. Bar graphs represent means  $\pm$  SD of three biological replicates (unless stated otherwise) with individual data points displayed. \* $P < 0.05$ , \*\* $P < 0.01$ , \*\*\* $P < 0.001$ , \*\*\*\* $P < 0.0001$  (Student's *t* test).



subunits were therefore overexpressed alone and in combination in HPV- C33A cervical cancer cells. Expression of Kir6.2 alone had no impact on the proliferation or colony-forming ability of the cells (Fig. 6A–C). Whilst SUR1 overexpression did result in a small

increase in anchorage-dependent and anchorage-independent colony formation, a significantly greater increase was observed when both subunits were overexpressed in combination (Fig. 6A–C). Together, these data indicate that  $K_{ATP}$  channel activity is

**Fig. 4 The E7 oncoprotein is responsible for the increase in SUR1 expression.** **A, B** Relative *ABCC8* mRNA expression measured by RT-qPCR in **(A)** HeLa and SiHa cells and **(B)** HPV18+ primary keratinocytes co-transfected with E6- and E7-specific siRNA. Samples were normalised against *U6* mRNA levels. Successful knockdown was confirmed by analysing *E6* and *E7* mRNA levels. **C, D** Expression levels of *ABCC8* mRNA measured by RT-qPCR in **(C)** C33A cells and **(D)** NHKs transfected with GFP-tagged HPV18 oncoproteins. Samples were normalised against *U6* mRNA levels and data is presented relative to the GFP-transfected control. Successful transfection was confirmed by immunofluorescence analysis (not shown). **E** Relative expression of *ABCC8* mRNA in C33A cells stably-expressing HA-tagged HPV18 oncoproteins measured by RT-qPCR. Samples were normalised against *U6* mRNA levels. Expression of oncoproteins was confirmed by western blot. **F** Mean DiBAC<sub>4</sub>(3) fluorescence levels in C33A cells after transfection of FLAG-tagged HPV18 E7 and treatment with either DMSO or glibenclamide (10 μM). Samples were normalised to the pcDNA3-transfected control. **G** Mean DiBAC<sub>4</sub>(3) fluorescence levels in C33A cells after co-transfection of FLAG-tagged HPV18 E7 and SUR1-specific siRNA. Samples were normalised to the pcDNA3/scramble-transfected control. **H** Mean DiBAC<sub>4</sub>(3) fluorescence levels in HeLa and SiHa cells after transfection of HPV E7-specific siRNA. Samples were normalised to the scramble control. Bars represent means ± SD of three biological replicates with individual data points displayed. *Ns* not significant, \**P* < 0.05, \*\**P* < 0.01, \*\*\**P* < 0.001, \*\*\*\**P* < 0.0001 (Student's *t* test).

pro-proliferative, and that the reduction in cell growth observed herein following channel inhibition or knockdown is likely not solely due to a loss of HPV oncoprotein expression.

#### **K<sub>ATP</sub> channel activity regulates progression through the G1/S phase transition**

To further evaluate the impact of reduced K<sub>ATP</sub> channel activity on cell proliferation, we assessed the cell cycle distribution of HPV+ cervical cancer cells using flow cytometry after blockade of K<sub>ATP</sub> channel activity. We felt this to be particularly pertinent as K<sub>ATP</sub> channel inhibition has been shown to result in a G1 phase arrest in glioma and breast cancer cell lines [30, 31]. In line with this, a significant increase in the proportion of cells in G1 phase was observed after both pharmacological inhibition of channel activity and siRNA-mediated SUR1 silencing in both HPV16+ and HPV18+ cervical cancer cells (Fig. 7A, B). As cyclins are key regulators of cell cycle progression, we also analysed their expression after glibenclamide treatment or suppression of SUR1 levels. We detected significant decreases in expression at both the mRNA and protein level of cyclin D1 (*CCND1*) and cyclin E1 (*CCNE1*), both of which regulate progression through G1 and the transition into S phase (Fig. 7C–F). This was consistent across both cell lines and treatments. In contrast, we observed only minimal changes in cyclin A2 (*CCNA2*) levels and no effect on cyclin B1 (*CCNB1*) expression at the mRNA level (Fig. 7C, D), with similar observations at the protein level (Fig. 7E, F). Together, these data suggest that K<sub>ATP</sub> channels drive proliferation by regulating the G1/S phase transition.

#### **K<sub>ATP</sub> channels are not required for the survival of cervical cancer cells**

We also wanted to investigate the impact of channel inhibition on the survival of HPV+ cervical cancer cells. Increased levels of apoptosis have been reported in some cancer types after K<sub>ATP</sub> channel blockade [29, 31, 32]. However, we failed to detect any increase in the cleavage of either poly(ADP) ribose polymerase (PARP) or caspase 3, both key indicators of the induction of apoptosis (Fig. S5A). Further, we also failed to observe an increase in either early or late apoptosis via Annexin V staining of exposed phosphatidylserine on the plasma membrane (Fig. S5B), thus confirming that K<sub>ATP</sub> channel inhibition alone does not impact upon the survival of HPV+ cervical cancer cells.

#### **K<sub>ATP</sub> channels contribute towards the activation of MAPK/AP-1 signalling**

We next wanted to gain an understanding into the mechanism by which K<sub>ATP</sub> channels promote proliferation in HPV+ cervical cancer cells. MAPK signalling is known to be a crucial driver of cell proliferation [49], and K<sub>ATP</sub> channel opening can lead to activation of the MAP kinase ERK1/2 [50, 51], so we therefore analysed ERK1/2 phosphorylation levels following stimulation of HPV+ cervical cells with diazoxide. This revealed a significant increase in ERK1/2 phosphorylation post-stimulation, which was reversed following

the addition of the MEK1/2 inhibitor U0126 (Fig. 8A). In addition, an increase in HPV18 E7 protein levels was observed, consistent with prior experiments; this was also reduced with U0126 treatment. Interestingly, an increase in both the phosphorylation and total protein expression of the AP-1 family member cJun was observed. AP-1 transcription factors are composed of dimers of proteins belonging to the Jun, Fos, Maf and ATF sub-families, and can regulate a wide variety of cellular processes, including proliferation, survival and differentiation [52]. This indicates that cJun/AP-1 could be a downstream target of ERK1/2 following K<sub>ATP</sub> channel stimulation.

To confirm these observations, overexpression of both K<sub>ATP</sub> channel subunits in combination was performed. This similarly resulted in increased ERK1/2 phosphorylation, increases in both cJun phosphorylation and total protein levels, as well as enhanced E7 expression (Fig. 8B). As before, these increases were reversed, in part, by the addition of U0126. To confirm that the changes in expression and phosphorylation of cJun corresponded to alterations in AP-1 activity, we employed a luciferase reporter construct containing three tandem AP-1 binding sites [53, 54]. K<sub>ATP</sub> channel overexpression led to a ~4 fold increase in relative AP-1 activity, which was significantly reduced in the presence of U0126 (Fig. 8C).

Following this, we performed assays to answer the question of whether the pro-proliferative effects of K<sub>ATP</sub> channels are mediated by this MAPK/AP-1 signalling axis. We observed an increase in the proliferation and colony-forming ability of HeLa cells following overexpression of K<sub>ATP</sub> channel subunits, which was reversed through MEK1/2 inhibition (Fig. 8D, E).

Next, we investigated the impact of reducing K<sub>ATP</sub> channel activity on AP-1 activity. Concordant with earlier data, a ~30% reduction in AP-1 activity was observed in HeLa cells following either glibenclamide treatment or transfection of SUR1-specific siRNA, as measured using a luciferase reporter assay (Fig. 8F, G). To investigate whether modulation of K<sub>ATP</sub> channel activity affected recruitment of cJun/AP-1 to the HPV URR, we performed ChIP-qPCR analysis using primers spanning the two AP-1 binding sites within the HPV18 URR, one in the enhancer region and one in the promoter [54]. This revealed that SUR1 knockdown reduced cJun recruitment to both binding sites within the viral URR, highlighting the critical role K<sub>ATP</sub> channels may have in regulating oncoprotein expression (Fig. 8H).

To further confirm our observations, we employed a dominant-negative JunD construct ( $\Delta$ JunD): this encodes a truncated form of JunD which is able to dimerise with other AP-1 family members, yet lacks a transcriptional activation domain. Previous studies in our lab have validated that  $\Delta$ JunD expression almost completely abolishes AP-1 activity [54]. Transfection of this construct resulted in a decrease in diazoxide-induced HPV oncoprotein expression (Fig. 8I).

Finally, we examined whether the reintroduction of active cJun would be able to rescue the proliferation defect of HeLa cells transfected with SUR1-specific siRNA. This revealed a significant increase in both proliferation and colony-forming

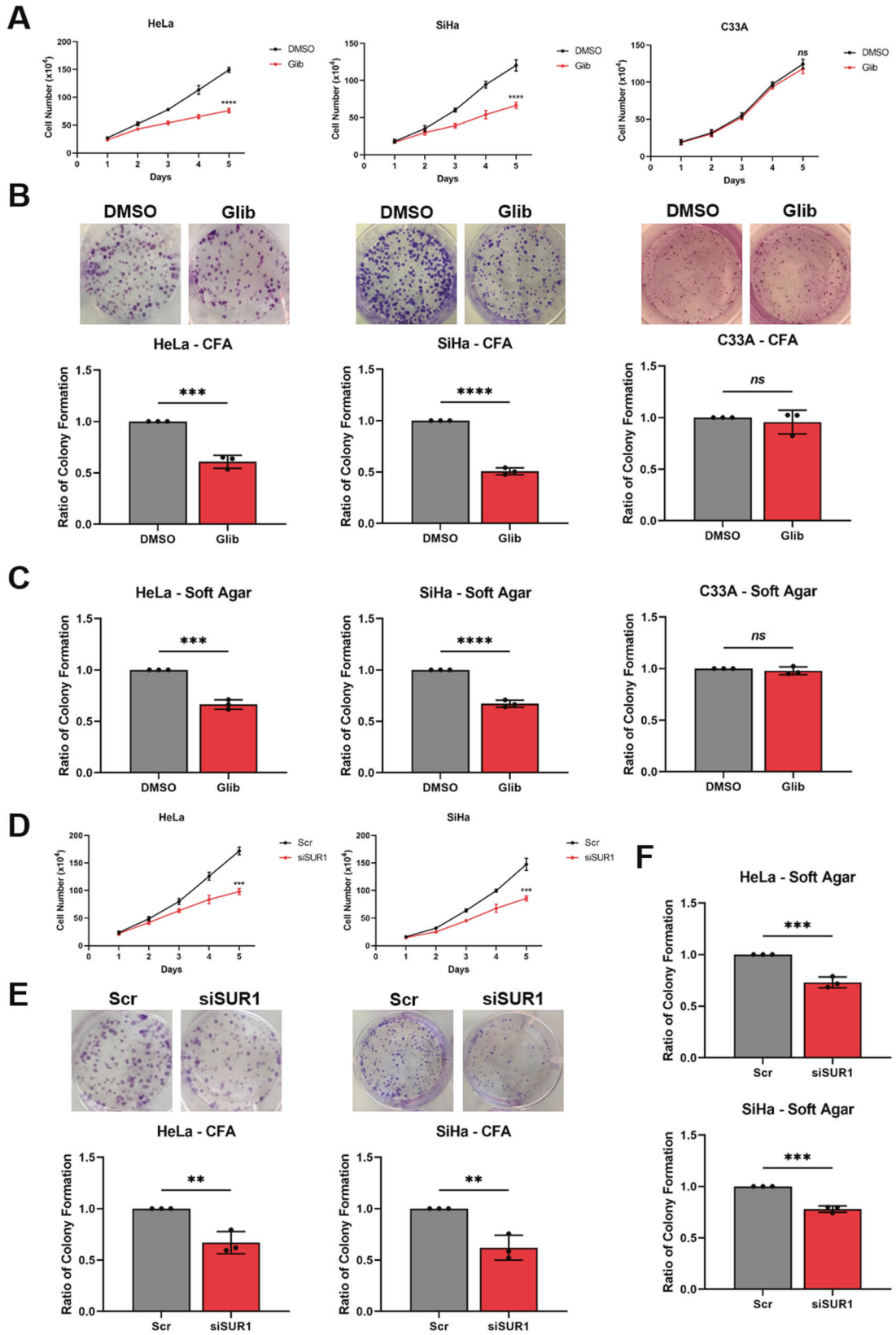


**Fig. 5**  $K_{ATP}$  channels drive proliferation in cervical cancer cells. **A–C** Growth curve analysis (**A**) colony formation assay (to measure anchorage-dependent growth) (**B**) and soft agar assay (to measure anchorage-independent growth) (**C**) of HeLa, SiHa and C33A cells after treatment with DMSO or glibenclamide (10  $\mu$ M) for 24 h. **D–F** Growth curve analysis (**D**), colony formation assay (**E**) and soft agar assay (**F**) of HeLa and SiHa cells after transfection of SUR1-specific siRNA. Data shown is means  $\pm$  SD of three biological replicates with individual data points displayed where appropriate. *Ns* not significant, \* $P < 0.05$ , \*\* $P < 0.01$ , \*\*\* $P < 0.001$ , \*\*\*\* $P < 0.0001$  (Student's *t* test).

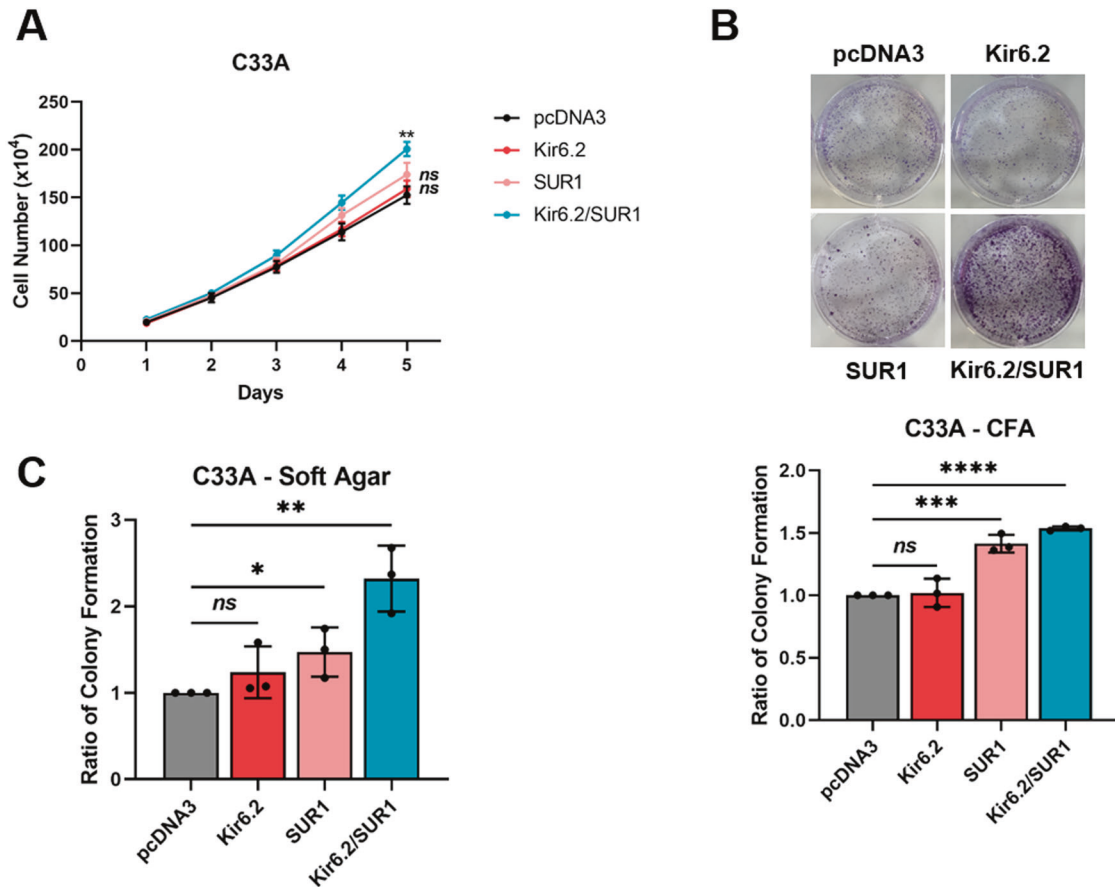


**Fig. 6**  $K_{ATP}$  channel overexpression is sufficient to stimulate proliferation in the absence of HPV. Growth curve analysis (A), colony formation assay (B) and soft agar assay (C) of C33A cells transfected with plasmids expressing HA-tagged Kir6.2 and/or SUR1. Data shown is means  $\pm$  SD of three biological replicates with individual data points displayed where appropriate. *Ns* not significant, \* $P < 0.05$ , \*\* $P < 0.01$ , \*\*\* $P < 0.001$ , \*\*\*\* $P < 0.0001$  (Student's *t* test).

ability following expression of a constitutively-active form of cJun, in which the two key phosphorylatable residues S63 and S73 are mutated to aspartic acid to mimic phosphorylation (S63/73D) (Fig. 8J, K) [55–57]. The rescue was incomplete however, illustrating that cJun/AP-1 is likely one of multiple targets downstream of  $K_{ATP}$  channel-induced ERK1/2 signalling. Taken together, these data indicate that  $K_{ATP}$  channel activity activates MAPK and AP-1 signalling to drive proliferation and oncoprotein expression.

#### $K_{ATP}$ channels drive proliferation in vivo

To confirm our in vitro observations, we performed tumourigenicity experiments using SCID mice. Animals were subcutaneously injected with HeLa cells stably expressing either a non-targeting shRNA or a SUR1-specific shRNA. Tumour development was monitored, revealing rapid growth in the HeLa shNTC control group, as expected (Fig. 9A). However, a significant delay in the growth of tumours in all mice injected with SUR1 knockdown cells compared to the shNTC controls was observed (Fig. 9A). To quantify this delay in growth, the period of time between injection of tumours and growth to a set volume ( $250 \text{ mm}^3$ ) was calculated. This revealed that the SUR1-depleted tumours took an additional 11 days on average to reach an equivalent size (Fig. 9B). Further, animals bearing SUR1-depleted tumours displayed significantly prolonged survival, with one mouse remaining alive at the conclusion of the study (Fig. 9C). Together, these data demonstrate that  $K_{ATP}$  channels drive the growth of HPV+ cervical cancer cell xenografts.

#### DISCUSSION

It is vital to identify virus-host interactions that are critical for HPV-mediated transformation as, despite the availability of prophylactic vaccines, there are currently no effective anti-viral treatments for HPV-associated disease. Here, we identify a novel host factor, the ATP-sensitive potassium ion ( $K_{ATP}$ ) channel, as a crucial driver of cell proliferation in HPV+ cervical cancer (Fig. 10). Inhibition of  $K_{ATP}$  channels, through either siRNA-mediated knockdown of individual subunits or pharmacological blockade using licenced inhibitors, significantly impedes proliferation and cell cycle progression. HPV is able to promote  $K_{ATP}$  channel activity via E7-mediated upregulation of the SUR1 subunit; this is observed in both cervical disease and cervical cancer tissue, as well as in vitro primary cell culture models of the HPV life cycle. As such, we believe that the clinically available inhibitors of  $K_{ATP}$  channels could constitute a potential novel therapy for HPV+ cervical cancer.

A growing number of viruses have been shown to modulate or require the activity of host ion channels [39]. Indeed, several viruses encode their own ion channels, termed 'viro-porins', including the HPV E5 protein [58–60]. Together, this underlines the importance of regulating host ion channel homeostasis during infection. Until recently however, much research in this field had focussed on RNA viruses, but recent work in our laboratories has highlighted roles for host chloride, potassium and calcium ion channels during BK polyomavirus (BKPyV), Merkel cell polyomavirus (MCPyV) and Kaposi's sarcoma-associated herpesvirus (KSHV) infection [61–63]. Importantly, this study is the first to our

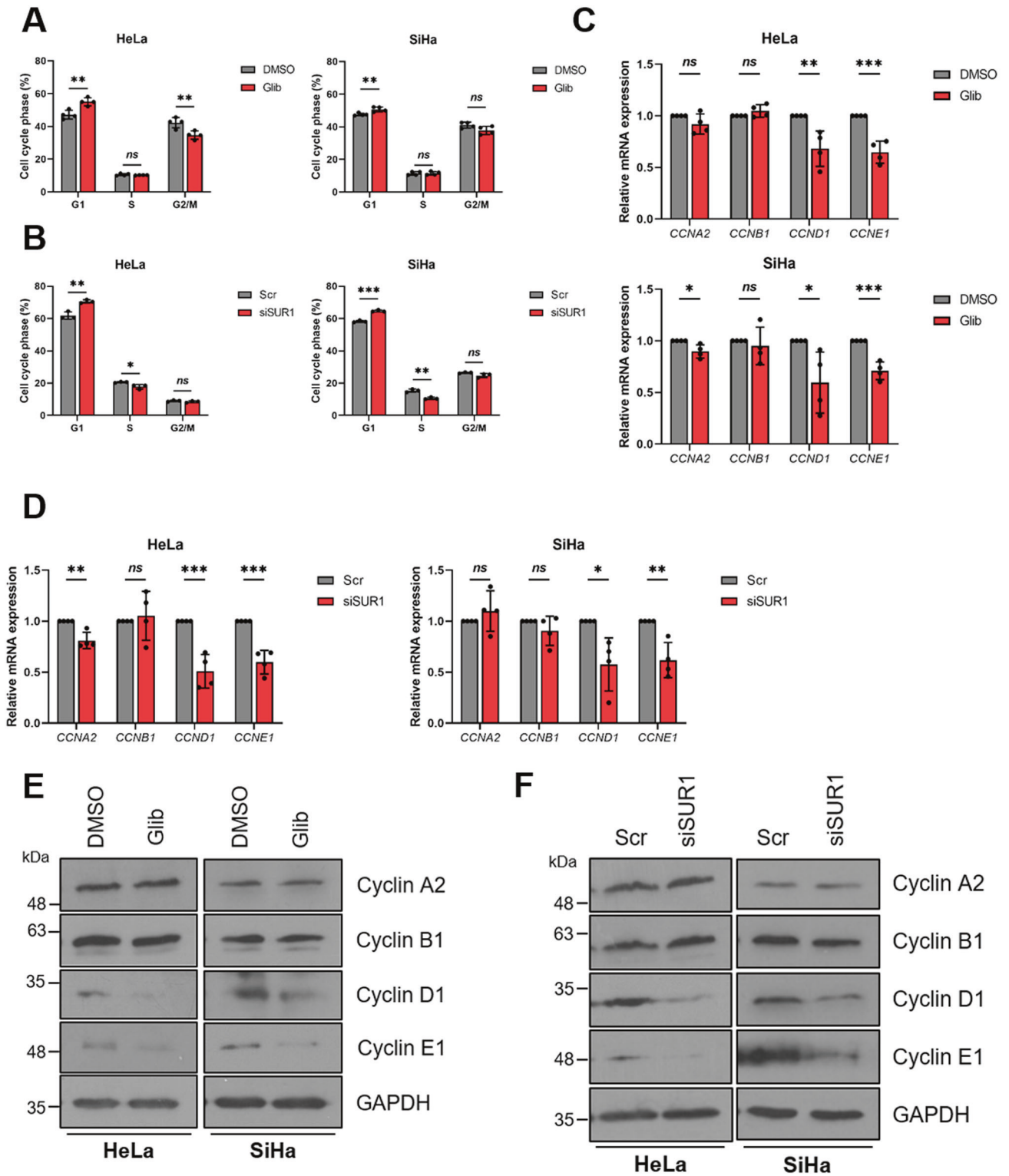
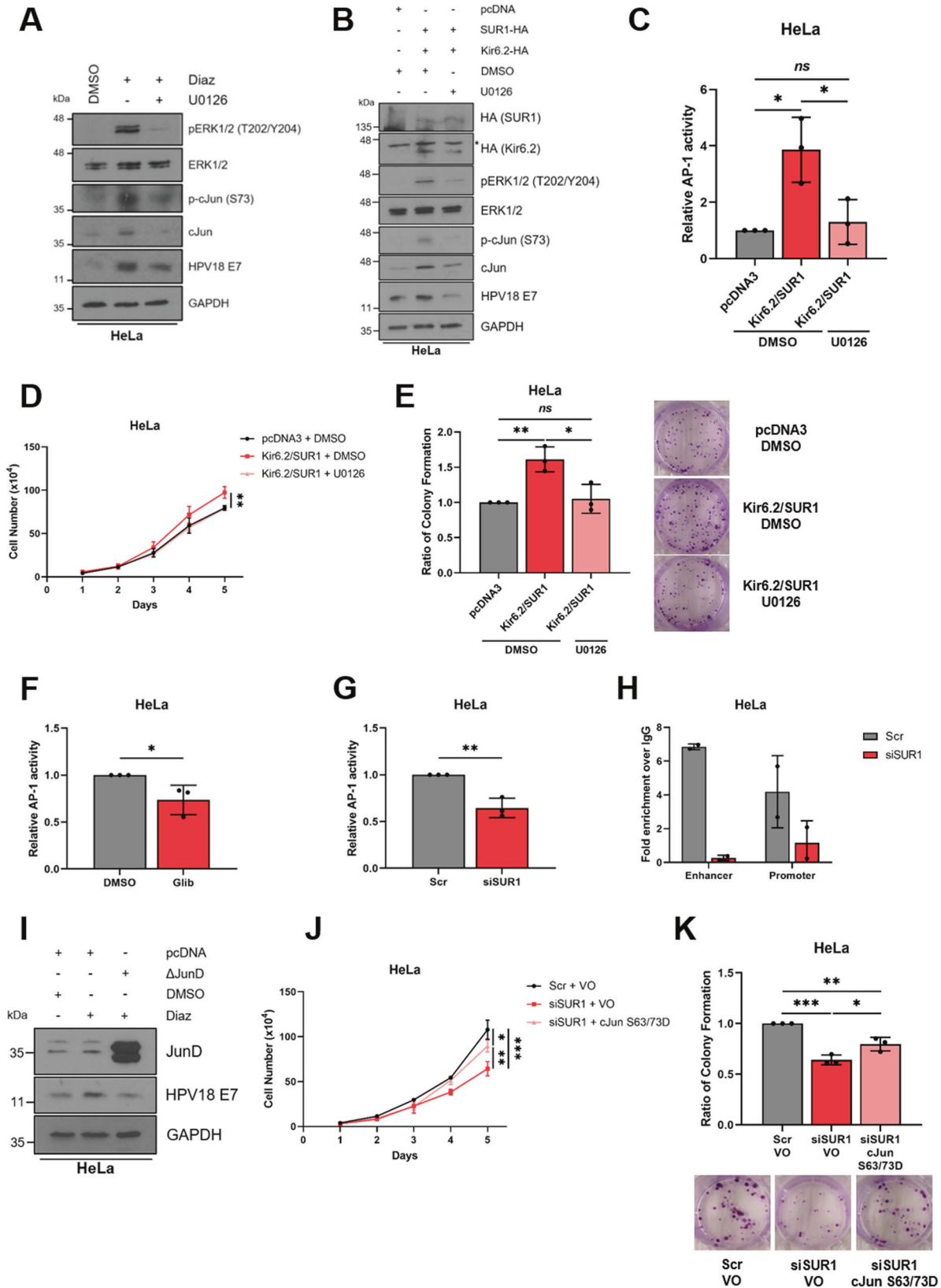


**Fig. 7**  $K_{ATP}$  channel activity regulates progression through the G1/S phase transition. **A, B** Flow cytometry analysis of cell cycle phase distribution of HeLa and SiHa cells after (A) treatment with either DMSO or glibenclamide (25  $\mu$ M) for 48 h ( $n = 4$ ) and (B) transfection of SUR1-specific siRNA. **C, D** mRNA expression levels of cyclins in HeLa and SiHa cells after (C) treatment with either DMSO or glibenclamide (10  $\mu$ M) for 24 h ( $n = 4$ ) or (D) transfection of SUR1-specific siRNA ( $n = 4$ ) measured by RT-qPCR. Samples were normalised against *U6* mRNA levels and data is displayed relative to the appropriate control. **E, F** Representative western blots of cyclin proteins in HeLa and SiHa cells after (E) treatment with either DMSO or glibenclamide (10  $\mu$ M) for 24 h or (F) transfection of SUR1-specific siRNA. GAPDH served as a loading control. Bars represent means  $\pm$  SD of three biological replicates (unless stated otherwise) with individual data points displayed. *Ns* not significant, \* $P < 0.05$ , \*\* $P < 0.01$ , \*\*\* $P < 0.001$  (Student's *t* test).



knowledge to explicitly demonstrate modulation of ion channel activity by HPV, and that this can contribute to host cell transformation. Although a previous study indicated that  $K_{ATP}$  channels are expressed in cervical cancer, no attempt was made to attribute this to HPV-mediated upregulation and the  $K_{ATP}$

channels found to be present were in fact comprised of Kir6.2 and the alternative regulatory subunit SUR2 [33]. Here, we found no evidence for expression of the SUR2A isoform, and SUR2B expression was not significantly increased in any of the HPV+ cell lines examined. Further, our functional analyses demonstrated

**Fig. 8**  $K_{ATP}$  channels drive proliferation by contributing towards the activation of MAPK/AP-1 signalling. **A, B** Representative western blots of phospho-ERK1/2, ERK1/2, phospho-cJun, cJun and E7 in HeLa cells either **(A)** serum starved for 24 h prior to treatment with diazoxide (50  $\mu$ M), with and without the MEK1/2 inhibitor U0126 (20  $\mu$ M), for 24 h or **(B)** transfected with plasmids expressing HA-tagged Kir6.2 and SUR1, with and without U0126 treatment (20  $\mu$ M). \* denotes the presence of a non-specific band. GAPDH served as a loading control. **C** Relative firefly luminescence in HeLa cells co-transfected with plasmids expressing HA-tagged Kir6.2 and SUR1 and an AP-1-driven reporter construct. Cells were also treated with DMSO or the MEK1/2 inhibitor U0126 (20  $\mu$ M) for 24 h. Luminescence values were normalised against *Renilla* luciferase activity. **D, E** Growth curve analysis **(D)** and colony formation assay **(E)** of HeLa cells after co-transfection with plasmids expressing HA-tagged Kir6.2 and SUR1 and treatment with DMSO or U0126 (20  $\mu$ M) for 24 h. **F, G** Relative firefly luminescence in HeLa cells transfected with an AP-1-driven reporter plasmid and either **(F)** treated with glibenclamide (10  $\mu$ M) or **(G)** transfected with SUR1-specific siRNA. Luminescence values were normalised against *Renilla* luciferase activity and data is displayed relative to the appropriate control. **H** ChIP-qPCR analysis of cJun binding to the HPV18 URR in HeLa cells transfected with SUR1-specific siRNA. Chromatin was prepared from HeLa cells and cJun immunoprecipitated using an anti-cJun antibody, followed by qPCR using primers specific to AP-1 binding sites in the HPV18 URR. cJun binding is presented as a fold increase over IgG binding ( $n = 2$ ). **I** Representative western blots for JunD, E6 and E7 expression in HeLa cells treated with diazoxide (50  $\mu$ M), with and without transfection of a plasmid expressing  $\Delta$ JunD. Cells were serum-starved for 24 h prior to treatment. GAPDH served as a loading control. **J, K** Growth curve analysis **(J)** and colony formation assay **(K)** of HeLa cells after co-transfection with SUR1-specific siRNA and a plasmid expressing a constitutively-active form of cJun (S63/73D). Bars represent means  $\pm$  SD of three biological replicates (unless stated otherwise) with individual data points displayed where appropriate. *Ns* not significant, \* $P < 0.05$ , \*\* $P < 0.01$ , \*\*\* $P < 0.001$  (Student's *t* test).

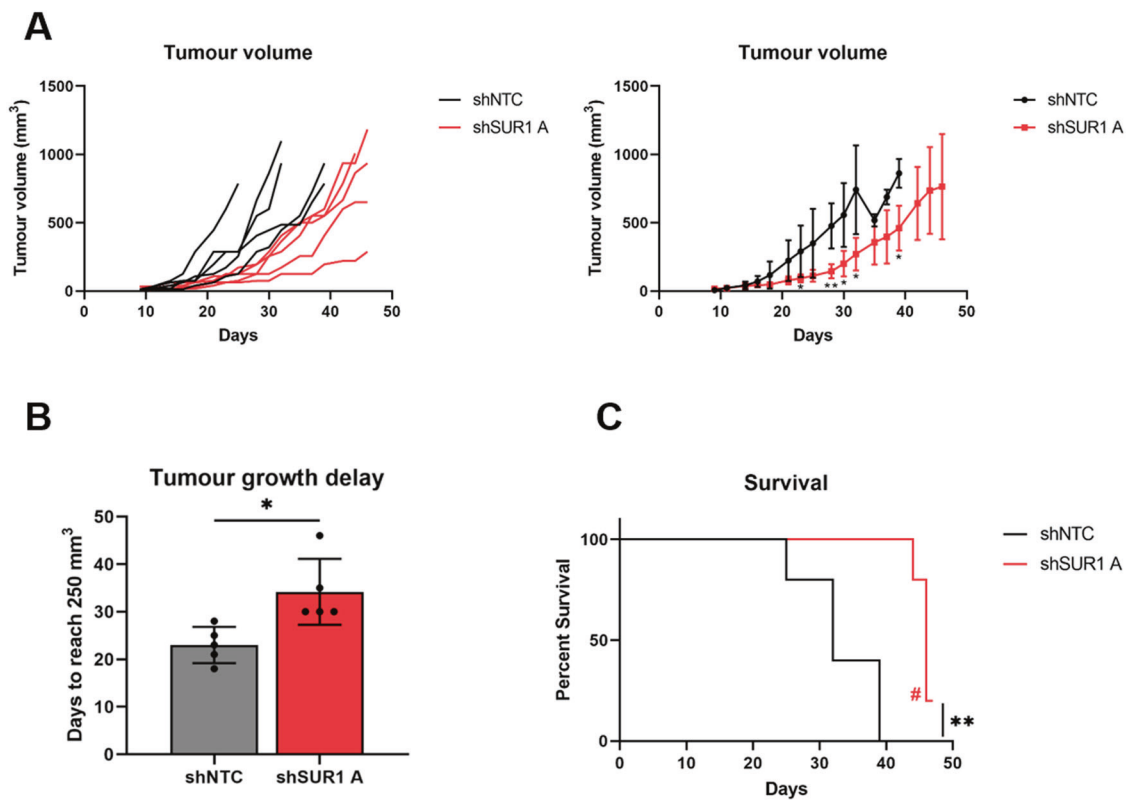


**Fig. 9**  $K_{ATP}$  channels drive proliferation in an in vivo mouse model. **A** Tumour growth curves for mice implanted with HeLa cells stably expressing either a non-targetting (shNTC) or an SUR1-specific shRNA (shSUR1 A). Tumour volume was calculated using the formula  $V = 0.5 \cdot L \cdot W^2$ . Both individual curves for each replicate (left) and curves representing mean values  $\pm$  SD of five mice per group (right) are displayed. **B** Tumour growth delay, calculated as the period of time between injection of tumours and growth to a set volume (250 mm<sup>3</sup>). Bars represent means  $\pm$  SD of five biological replicates with individual data points displayed. \* $P < 0.05$  (Student's *t* test). **C** Kaplan-Meier survival curve of mice bearing shNTC and shSUR1 A tumours. Indicates that one mice remained alive at the conclusion of the study. \*\* $P < 0.01$  (log-rank (Mantel-Cox) test).

that SUR2B has no impact on the proliferation of HPV+ cervical cancer cells.

More widely, few reports exist of a dependence on host  $K_{ATP}$  channel activity for viral replication. One study identified that inhibition of  $K_{ATP}$  channels via glibenclamide treatment precludes HIV cell entry but, in contrast, cardiac  $K_{ATP}$  channel activity was found to be detrimental to Flock House virus (FHV) infection of *Drosophila* [64, 65]. Significantly however, no evidence exists to suggest that either of these viruses actively modulate the gating and/or expression of these channels, as we have demonstrated for HPV here.

In order to confirm that the effects on HPV oncoprotein expression and proliferation observed during this study following SUR1 knockdown were due to decreased  $K_{ATP}$  channel activity, silencing of the pore-forming Kir6.2 subunit was also performed. We felt this pertinent as recent studies have concluded that the oncogenic activities of SUR1 in non-small cell lung carcinoma (NSCLC) are independent of  $K_{ATP}$  channel activity [66, 67], and SUR1 is reported to have a supplementary role in regulating the activity of an ATP-sensitive, non-selective ion channel in astrocytes [68]. However, we observed almost identical effects on cell proliferation and HPV oncoprotein expression following Kir6.2

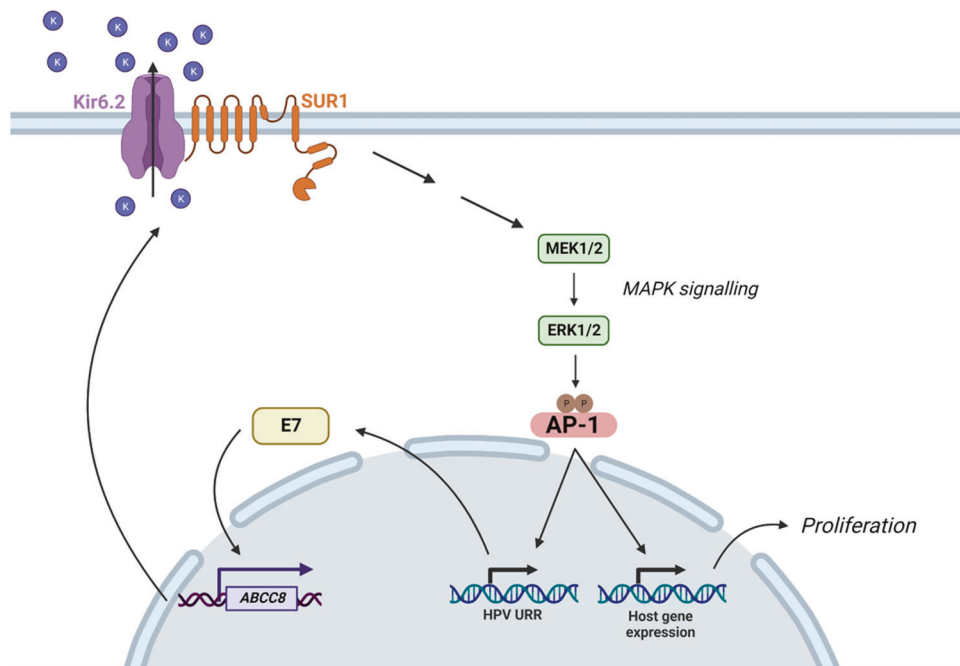


**Fig. 10 Schematic demonstrating E7-mediated upregulation of K<sub>ATP</sub> channel expression and activity.** HPV E7 upregulates expression of *ABCC8*, the gene encoding SUR1 which constitutes the regulatory subunit of K<sub>ATP</sub> channels. Increased K<sub>ATP</sub> channel activity contributes towards the activation of MAPK and AP-1 signalling. This, in turn, drives transcription from the viral URR and changes in host gene expression which together stimulate proliferation. Figure created using BioRENDER.com.

knockdown, leading us to conclude that SUR1 does not act in a K<sub>ATP</sub> channel-independent manner in cervical cancer. This is supported by our overexpression data, in which a significant increase in the proliferative ability of HPV- C33A cells was only observed when both channel subunits were transfected. This also fits with the current assembly hypothesis for K<sub>ATP</sub> channels, whereby neither subunit can be trafficked beyond the endoplasmic reticulum unless fully assembled into hetero-octameric channels [69–71].

We observed that inhibition of K<sub>ATP</sub> channels, through either pharmacological means or SUR1 knockdown, resulted in an increase in the proportion of cells in G1 phase and, consistently, a decrease in cyclin D1 and E1 expression. This is in line with prior reports in other cell types [30, 31, 50]. Further, this fits with an increasing recognition of the importance of ion channels in the regulation of the cell cycle and cell proliferation [24–26, 28]. It is thought that cells undergo a rapid hyperpolarisation during progression through the G1-S phase checkpoint, for which K<sup>+</sup> efflux channels are particularly important [25, 26]. Our data indicates that, at least in cervical cancer, K<sub>ATP</sub> channels may contribute towards this hyperpolarisation event. Further, several K<sup>+</sup> channels demonstrate cell cycle-dependent variations in expression and/or activity [72–75]; whether this is the case for K<sub>ATP</sub> channels in HPV+ cancer cells warrants further analysis.

Ion channels represent ideal candidates for novel cancer therapeutics given the abundance of licensed and clinically available drugs targeting the complexes which could be repurposed if demonstrated to be effective [23]. We therefore investigated whether K<sub>ATP</sub> channel inhibition had a cytotoxic effect on cervical cancer cells. Somewhat surprisingly, given the impact on HPV oncoprotein expression, we did not observe any evidence for increased cell death following glibenclamide treatment. This is in contrast to previous experiments in gastric cancer, glioma and hepatocellular carcinoma cell lines [29, 31, 32], yet in agreement with observations in breast cancer cells [30]. These differences may potentially reflect the cell type-specific

roles of K<sub>ATP</sub> channels, or perhaps be a result of differing subunit compositions in the cell types analysed. It is also feasible that, as we did not observe total abolition of oncoprotein expression, the cervical cancer cells were able to continue proliferating, albeit at a significantly reduced rate. It may therefore be of interest to investigate whether in response to a more prolonged exposure to K<sub>ATP</sub> channel blockers, resulting in long-term suppression of E6/E7 expression, cervical cancer cells begin to exhibit an apoptotic or senescent phenotype. Following this, we performed *in vivo* tumourigenicity assays using cell lines stably expressing SUR1-specific shRNAs. We observed significant delays to tumour growth with cells displaying reduced SUR1 expression resulting in prolonged survival, thus providing validation for our earlier *in vitro* work. Given the clear impact suppression of K<sub>ATP</sub> channel activity has on the growth of HPV+ cervical cancer cells, further work is now warranted to confirm whether the licensed K<sub>ATP</sub> channel inhibitors could be repurposed and used alongside current therapies.

We revealed that the pro-proliferative effects of K<sub>ATP</sub> channels are mediated via activation of ERK1/2 and subsequently the AP-1 family member cJun. Previous reports have examined the importance of these signalling pathways in HPV infection and cervical cancer [46, 54, 76–79]. Indeed, a recent study elegantly showed a strong correlation between ERK1/2 activity and cervical disease progression, and highlighted the importance of ERK1/2 and AP-1 signalling for oncoprotein expression in both a life cycle model of HPV infection and using an oropharyngeal squamous cell carcinoma cell line [79]. Interestingly, this study additionally identified the AP-1 family members cFos and JunB as contributors towards oncogene transcription, whilst our own analysis has revealed that both cJun and JunD are upregulated in HPV18+ keratinocytes and cervical cancer cell lines [54, 79]. As AP-1 can be comprised of Jun family homodimers or heterodimers with Fos, ATF or MAF family proteins, further studies may be warranted to determine the most frequent makeup of AP-1 dimers in HPV+ cells [52].

In conclusion, we present evidence that host  $K_{ATP}$  channels play a crucial role in cervical carcinogenesis. Upregulation of the SUR1 subunit by HPV E7 contributes towards increased  $K_{ATP}$  channel activity, which in turn drives cell proliferation and progression through the G1/S phase checkpoint via MAPK/AP-1 signalling.  $K_{ATP}$  channels also promote HPV E6/E7 expression, thus establishing a positive feedback network. A complete characterisation of the role of  $K_{ATP}$  channels in HPV-associated disease is therefore now warranted in order to determine whether the licensed and clinically available inhibitors of these channels could constitute a potential novel therapy in the treatment of HPV-driven cancers.

## MATERIALS AND METHODS

### Cervical cancer cytology samples

Cervical cytology samples were obtained from the Scottish HPV Archive (<http://www.shine.mvm.ed.ac.uk/archive.shtml>), a biobank of over 20,000 samples designed to facilitate HPV-associated research. The East of Scotland Research Ethics Service has given generic approval to the Scottish HPV Archive as a Research Tissue Bank (REC Ref 11/AL/0174) for HPV related research on anonymised archive samples. Samples are available for the present project through application to the Archive Steering Committee (HPV Archive Application Ref 0034). RNA was extracted from the samples using TRIzol® Reagent (ThermoFisher Scientific) and analysed as described.

### Plasmids and siRNA

Expression vectors for  $\Delta$ JunD, HA-tagged Kir6.2 and SUR1, and GFP-tagged HPV18 E6 and E7 have been described previously [54, 80, 81]. The FLAG-tagged HPV18 E7 expression vector was cloned from the above GFP-HPV18 E7 vector. Luciferase reporter constructs for the HPV18 URR and the HPV16 URR were kind gifts from Prof Felix Hoppe-Seyler (German Cancer Research Center (DKFZ)) and Dr Iain Morgan (Virginia Commonwealth University (VCU)) respectively [77, 82]. The HA-tagged cJun S63/73D expression vector was kindly provided by Dr Hans van Dam (Leiden University Medical Centre (LUMC)) [83]. The AP-1 luciferase reporter has been described previously [53].

For siRNA experiments, pools of four siRNAs specific to *ABCC8* (FlexiTube GeneSolution GS6833), *ABCC9* (FlexiTube GeneSolution GS10060), and *KCNJ11* (FlexiTube GeneSolution GS3767) were purchased from Qiagen. HPV16 E6 siRNA (sc-156008) and HPV16 E7 siRNA (sc-270423) were purchased from Santa Cruz Biotechnology (SCBT). HPV18 E6 siRNAs were purchased from Dharmacon (GE Healthcare) and had the following sequences: 5'-CUAACACUGGGUUUAUACAA-3' and 5'-CTAACTAACACTGGGTAT-3'. HPV18 E7 siRNA were as previously described and were a kind gift from Prof Eric Blair (University of Leeds) [84, 85]. A final siRNA concentration of 25 nM was used in all cases.

### $K^+$ channel modulators and small molecule inhibitors

The  $K_{ATP}$  inhibitors glibenclamide and tolbutamide were purchased from Sigma and used at final concentrations of 10  $\mu$ M and 200  $\mu$ M unless stated otherwise. The  $K^+$  channel blockers tetraethylammonium (TEA), quinine, quinidine, 4-aminopyridine (4-AP), ruthenium red (RR), apamin, bupivacaine hydrochloride (BupHCl) and margatoxin were purchased from Sigma and used at the stated concentrations. The  $K_{ATP}$  channel activator diazoxide was purchased from Cayman Chemical and used at 50  $\mu$ M unless stated otherwise. The MEK1/2 inhibitor U0126 (Calbiochem) was used at 20  $\mu$ M. Staurosporine (Calbiochem) was used at a final concentration of 1  $\mu$ M.

### Cell culture

HeLa (HPV18+ cervical epithelial adenocarcinoma cells), SW756 (HPV18+ cervical squamous carcinoma cells), SiHa (HPV16+ cervical squamous carcinoma cells), CaSki (HPV16+ cervical squamous carcinoma cells) and C33A (HPV- cervical squamous carcinoma) cells obtained from the ATCC were grown in DMEM supplemented with 10% FBS (ThermoFisher Scientific) and 50 U/mL penicillin/streptomycin (Lonza). HEK293TT cells were kindly provided by Prof Greg Towers (University College London (UCL)) and grown as above.

Neonate foreskin tissues were obtained from local General Practice surgeries and foreskin keratinocytes isolated under ethical approval no 06/Q1702/45. Cells were maintained in serum-free medium (SFM; Gibco) supplemented with 25  $\mu$ g/mL bovine pituitary extract (Gibco) and 0.2 ng/mL recombinant EGF (Gibco). The transfection of primary NHKs to generate

HPV18+ keratinocytes was performed as described previously [86]. All cells were cultured at 37 °C and 5% CO<sub>2</sub>.

All cells were negative for mycoplasma during this investigation. Cell identity was confirmed by STR profiling.

### Organotypic raft culture

NHKs and HPV18+ keratinocytes were grown in organotypic raft cultures by seeding the keratinocytes onto collagen beds containing J2-3T3 fibroblasts [86]. Once confluent, the collagen beds were transferred onto metal grids and fed from below with FCS-containing E media without EGF. The cells were allowed to stratify for 14 days before fixing with 4% formaldehyde. The rafts were paraffin-embedded and 4  $\mu$ m tissue sections prepared (Propath UK Ltd.). For analysis of SUR1 expression, the formaldehyde-fixed raft sections were treated with the sodium citrate method of antigen retrieval. Briefly, sections were boiled in 10 mM sodium citrate with 0.05% Tween-20 for 10 min. Sections were incubated with a polyclonal antibody against SUR1 (PA5-50836, ThermoFisher Scientific) and immune complexes visualised using Alexa 488 and 594 secondary antibodies (Invitrogen). The nuclei were counterstained with DAPI and mounted in Prolong Gold (Invitrogen).

### Transfection of cancer cell lines

Transient transfections were performed using Lipofectamine 2000 (ThermoFisher Scientific). A ratio of nucleic acid to Lipofectamine 2000 of 1:2 was used for both DNA and siRNA. Transfections were performed overnight in OptiMEM I Reduced Serum Media (ThermoFisher Scientific). Subsequent analyses were performed at 48 h (plasmid DNA) or 72 h (siRNA) post-transfection.

### Generation of stable cell lines

HEK293TT cells were co-transfected with the packaging plasmids pCRV1-NLGP and pCMV-VSV-G alongside either a pZIP-hEF1 $\alpha$ -non-targeting shRNA construct or one of two pZIP-hEF1 $\alpha$ -SUR1 shRNA constructs (purchased from TransOMIC). At 48 h post-transfection, virus-containing media was harvested and passed through a 0.45  $\mu$ m filter to remove cell debris. To perform lentiviral transductions, culture media was removed from HeLa cells seeded 24 h earlier and replaced with virus-containing media. Cells were incubated overnight before removing virus and replacing with complete DMEM. At 48 h post-transduction, cells were passaged as appropriate and treated with 1  $\mu$ g/mL puromycin in culture media for 48 h to select for transduced cells. Fluorescence-associated cell sorting (FACS) was used to partition individual surviving cells into wells of 96-well culture plates in order to generate monoclonal cell lines.

HPV- C33A cells stably expressing HPV18 E6 or E7 were generated as previously described [18].

### Western blot analysis

Equal amounts of protein from cell lysates were resolved by molecular weight using 8–15% SDS-polyacrylamide gels as appropriate. Separated proteins were transferred to Hybond™ nitrocellulose membranes (GE Healthcare) using a semi-dry method (Bio-Rad Trans-Blot® Turbo™ Transfer System). Membranes were blocked in 5% skimmed milk powder in tris-buffered saline-0.1% Tween-20 (TBS-T) for 1 h at room temperature before probing with antibodies specific for HPV16 E6 (GTX132686, GeneTex, Inc.), HPV16 E7 (ED17: sc-6981, SCBT), HPV18 E6 (G-7: sc-365089, SCBT), HPV18 E7 (8E2: ab100953, abcam), HA (3724, Cell Signalling Technology (CST)), cyclin A (B-8: sc-271682, SCBT), cyclin B1 (12231, CST), cyclin D1 (ab134175, abcam), cyclin E1 (20808, CST), PARP (9542, CST), caspase-3 (9662, CST), cleaved caspase-3 (D175) (9664, CST), phospho-ERK1/2 (T202/Y204) (9101, CST), ERK1/2 (9102, CST), phospho-cJun (S73) (3270, CST), cJun (9165, CST), JunD (5000, CST) and GAPDH (G-9: sc-365062, SCBT). Primary antibody incubations were performed overnight at 4 °C. The appropriate HRP-conjugated secondary antibodies (Jackson ImmunoResearch) were used at a 1:5000 dilution. Blots were visualised using ECL reagents and CL-Xposure™ film (ThermoFisher Scientific). A minimum of three biological repeats were performed in all cases and representative blot images are displayed.

### RNA extraction and reverse transcription-quantitative PCR (RT-qPCR)

Total RNA was extracted from cells using the E.Z.N.A.® Total RNA Kit I (Omega Bio-Tek) following the provided protocol for RNA extraction from

cultured cells. The concentration of eluted RNA was determined using a NanoDrop™ One spectrophotometer (ThermoFisher Scientific). RT-qPCR was performed using the GoTaq® 1-Step RT-qPCR System (Promega) with an input of 50 ng RNA. Reactions were performed using a CFX Connect Real-Time PCR Detection System (Bio-Rad) with the following cycling conditions: reverse transcription for 10 min at 50 °C; reverse transcriptase inactivation/polymerase activation for 5 min at 95 °C followed by 40 cycles of denaturation (95 °C for 10 s) and combined annealing and extension (60 °C for 30 s). Data were analysed using the  $\Delta\Delta C_t$  method [87]. The primers used in this study are detailed in Table S1; *U6* expression was used for normalisation.

### Tissue microarray and immunohistochemistry

A cervical cancer tissue microarray (TMA) containing 39 cases of cervical cancer and 9 cases of normal cervical tissue (in duplicate) was purchased from GeneTex, Inc. (GTX21468). Slides were deparaffinised in xylene, rehydrated in a graded series of ethanol solutions and subjected to antigen retrieval in citric acid. Slides were blocked in normal serum and incubated in primary antibody (SUR1 (75-267, Antibodies Inc.)) overnight at 4 °C. Slides were then processed using the VECTASTAIN™ Universal Quick HRP Kit (PK-7800; Vector Laboratories) as per the manufacturer's instructions. Immunostaining was visualised using 3,3'-diaminobenzidine (Vector® DAB (SK-4100; Vector Laboratories)). Images were taken using an EVOS® FL Auto Imaging System (ThermoFisher Scientific) at  $\times 20$  magnification. SUR1 quantification was automated using ImageJ with the IHC Profiler plug-in [88, 89]. Histology scores (H-score) were calculated based on the percentage of positively stained tumour cells and the staining intensity grade. The staining intensities were classified into the following four categories: 0, no staining; 1, low positive staining; 2, positive staining; 3, strong positive staining. H-score was calculated by the following formula:  $(3 \times \text{percentage of strong positive tissue}) + (2 \times \text{percentage of positive tissue}) + (\text{percentage of low positive tissue})$ , giving a range of 0–300.

### Patch clamping

HeLa cells were seeded on coverslips in 12-well culture plates at 10–20% confluency to prevent cell-cell contact. Following attachment, cells were treated with DMSO, 10  $\mu\text{M}$  glibenclamide, 50  $\mu\text{M}$  diazoxide, or with both channel modulators in combination for 16 h. Following treatment, patch pipettes (2–4 M $\Omega$ ) were filled with pipette solution (5 mM HEPES-KOH pH 7.2, 140 mM KCl, 1.2 mM MgCl<sub>2</sub>, 1 mM CaCl<sub>2</sub>, 10 mM EGTA, 1 mM MgATP, 0.5 mM NaUDP) and culture media removed from cells and replaced with external solution (5 mM HEPES-KOH pH 7.4, 140 mM KCl, 2.6 mM CaCl<sub>2</sub>, 1.2 mM MgCl<sub>2</sub>). Whole cell patch clamp recordings were performed using an Axopatch 200B amplifier/Digidata 1200 interface controlled by Clampex 9.0 software (Molecular Devices). A series of depolarising steps, from –100 to +60 mV in 10 mV increments for 100 ms each, was applied to cells and the K<sup>+</sup> current measured. Analysis was performed using the data analysis package Clampfit 9.0 (Molecular Devices).

### Chromatin immunoprecipitation (ChIP)

After treatment as required, cells were processed for ChIP as previously described [81]. cJun was immunoprecipitated using a ChIP grade anti-cJun antibody (9165, CST) and each of the samples were also pulled down with an IgG isotype control to confirm antibody specificity. Pierce™ Protein A/G Magnetic Beads (ThermoFisher Scientific) were used to isolate antibody-chromatin complexes. Immunoprecipitated chromatin was then processed for quantitative PCR (qPCR) using primers covering the AP-1 binding sites within the HPV18 URR (sequences available upon request). Fold enrichment was calculated by comparing to the IgG isotype control.

### Luciferase reporter assays

Cells were transfected with plasmids expressing the appropriate firefly luciferase reporter (250 ng). 25 ng of a *Renilla* luciferase reporter construct (pRLTK) was used as an internal control for transfection efficiency. Samples were lysed in passive lysis buffer (Promega) and activity measured using a dual-luciferase reporter assay system (Promega). All assays were performed in triplicate, and each experiment was repeated a minimum of three times.

### Proliferation assays

For cell growth assays, cells were detached by trypsinisation after treatment as necessary and reseeded at equal densities in 12-well plates.

Cells were subsequently harvested every 24 h and manually counted using a haemocytometer.

For colony formation assays, cells were detached by trypsinisation after treatment as required and reseeded at 500 cells/well in six-well plates. Once visible colonies were noted, culture media was aspirated and cells fixed and stained in crystal violet staining solution (1% crystal violet, 25% methanol) for 15 min at room temperature. Plates were washed thoroughly with water to remove excess crystal violet and colonies counted manually.

For soft agar assays, 60 mm cell culture plates were coated with a layer of complete DMEM containing 0.5% agarose. Simultaneously, cells were detached by trypsinisation after treatment as required and resuspended at 1000 cells/mL in complete DMEM containing 0.35% agarose and added to the bottom layer of agarose. Once set, plates were covered with culture media and incubated for 14–21 days until visible colonies were observed. Colonies were counted manually.

### Cell cycle analysis

Cells were harvested and fixed overnight in 70% ethanol at –20 °C. Ethanol was removed by centrifugation at 500  $\times g$  for 5 min and cells washed twice in PBS containing 0.5% BSA. Cells were resuspended in 500  $\mu\text{L}$  0.5% BSA/PBS, treated with 1.25  $\mu\text{L}$  RNase A/T1 mix (ThermoFisher Scientific) and stained with 8  $\mu\text{L}$  1 mg/mL propidium iodide solution (Sigma) for 30 min at room temperature in the dark. Analysis was performed using a CytoFLEX S flow cytometer (Beckman Coulter).

### DiBAC assay

After treatment as necessary, the membrane potential-sensitive dye DiBAC<sub>4</sub>(3) (Bis-(1,3-Dibutylbarbituric Acid) Trimethine Oxonol; ThermoFisher Scientific) was added directly to culture media at a final concentration of 200 nM. Cells were incubated in the presence of the dye for 20 min at 37 °C in the dark. Cells were harvested by scraping and washed twice in PBS. Cells were resuspended in 500  $\mu\text{L}$  PBS for flow cytometry analysis. Analysis was performed using a CytoFLEX S flow cytometer (Beckman Coulter).

### Annexin V assay

Annexin V apoptosis assays were performed using the TACS® Annexin V-FITC Kit (Bio-Techne Ltd.). After treatment as required, cells were harvested by aspirating and retaining culture media (to collect detached apoptotic cells) with the remaining cells detached by trypsinisation. The retained media and trypsin cell suspension was combined and centrifuged at 500  $\times g$  for 5 min to pellet cells before washing once in PBS and pelleting again. Cells were incubated in 100  $\mu\text{L}$  Annexin V reagent (10  $\mu\text{L}$  10 $\times$  binding buffer, 10  $\mu\text{L}$  propidium iodide, 1  $\mu\text{L}$  Annexin V-FITC (diluted 1:25), 79  $\mu\text{L}$  ddH<sub>2</sub>O) for 15 min at room temperature protected from light. 400  $\mu\text{L}$  of 1 $\times$  binding buffer was then added before analysing using a CytoFLEX S flow cytometer (Beckman Coulter). Annexin V-FITC positive cells were designated as early apoptotic, whilst dual Annexin V-FITC/PI positive cells were designated as late apoptotic. Cells negative for both Annexin V and PI staining were considered to be healthy.

### In vivo tumourigenicity study

Female 6–8 week old SCID mice were purchased from Charles River Laboratories. All animal work was carried out under project license PP1816772. HeLa cells stably expressing either a non-targeting shRNA or a SUR1-specific shRNA were harvested, pelleted and resuspended in sterile PBS. Five mice were used per experimental group, with each injected subcutaneously with  $5 \times 10^5$  cells in 50  $\mu\text{L}$  PBS. Once palpable tumours had formed (~ 10 days), measurements for both groups were taken thrice weekly. After tumours reached 10 mm in either dimension, mice were monitored daily. Mice were sacrificed once tumours reached 15 mm in any dimension. No toxicity, including significant weight loss, was seen in any of the mice. Tumour volume was calculated with the formula  $V = 0.5 \times L \times W^2$ .

### Microarray analysis

For microarray analysis, a dataset consisting of 24 normal, 14 CIN1 lesions, 22 CIN2 lesions, 40 CIN3 lesions, and 28 cancer specimens was utilised. Microarray data was obtained from GEO database accession number GSE63514 [90].

## Statistical analysis

All *in vitro* experiments were performed a minimum of three times, unless stated otherwise, to ensure reproducibility and to allow statistical analyses to be performed. The sample size for the *in vivo* study was selected by assuming an expected mean survival of the control animal group of  $\sim 40 \pm 5$  days (based on previous experiments in the subcutaneous SCID/HeLa flank model) and that the shSUR1 tumours would survive an additional 10 days on average. In previous experiments, no animals have been lost prematurely due to toxicity. Assuming these effect sizes and variance, using 5 animals in each group and a significance level of 95% ( $\alpha$  error probability = 0.05), the power ( $1 - \beta$  error probability) to observe a difference between the experimental and control groups was  $\sim 80\%$ .

Data were analysed using a two-tailed, unpaired Student's *t* test performed using GraphPad PRISM 9.2.0 software, unless stated otherwise. Kaplan–Meier survival data was analysed using the log-rank (Mantel–Cox) test.

## DATA AVAILABILITY

All data generated or analysed during this study are included in this published paper and its supplementary information files.

## REFERENCES

- Graham SV. The human papillomavirus replication cycle, and its links to cancer progression: a comprehensive review. *Clin Sci (London, England : 1979)*. 2017;131:2201–21.
- Scarth JA, Patterson MR, Morgan EL, Macdonald A. The human papillomavirus oncoproteins: a review of the host pathways targeted on the road to transformation. *J General Virol*. 2021;102:001540.
- Stanley M. Pathology and epidemiology of HPV infection in females. *Gynecol Oncol*. 2010;117:55–10.
- Moody CA, Laimins LA. Human papillomavirus oncoproteins: pathways to transformation. *Nat Rev Cancer*. 2010;10:550–60.
- Munger K, Werness BA, Dyson N, Phelps WC, Harlow E, Howley PM. Complex formation of human papillomavirus E7 proteins with the retinoblastoma tumor suppressor gene product. *EMBO J*. 1989;8:4099–105.
- Dyson N, Howley PM, Munger K, Harlow E. The human papilloma virus-16 E7 oncoprotein is able to bind to the retinoblastoma gene product. *Science*. 1989;243:934–7.
- Boyer SN, Wazer DE, Band V. E7 protein of human papilloma virus-16 induces degradation of retinoblastoma protein through the ubiquitin-proteasome pathway. *Cancer Res*. 1996;56:4620–4.
- Scheffner M, Huibregtse JM, Vierstra RD, Howley PM. The HPV-16 E6 and E6-AP complex functions as a ubiquitin-protein ligase in the ubiquitination of p53. *Cell*. 1993;75:495–505.
- Gewin L, Myers H, Kiyono T, Galloway DA. Identification of a novel telomerase repressor that interacts with the human papillomavirus type-16 E6/E6-AP complex. *Genes Dev*. 2004;18:2269–82.
- Ganti K, Broniarczyk J, Manoubi W, Massimi P, Mittal S, Pim D, et al. The Human Papillomavirus E6 PDZ Binding Motif: From Life Cycle to Malignancy. *Viruses*. 2015;7:3530–51.
- Richards KH, Doble R, Wasson CW, Haider M, Blair GE, Wittmann M, et al. Human papillomavirus E7 oncoprotein increases production of the anti-inflammatory interleukin-18 binding protein in keratinocytes. *J Virol*. 2014;88:4173–9.
- Westrich JA, Warren CJ, Pyeon D. Evasion of host immune defenses by human papillomavirus. *Virus Res*. 2017;231:21–33.
- Morgan EL, Wasson CW, Hanson L, Kealy D, Pentland I, McGuire V, et al. STAT3 activation by E6 is essential for the differentiation-dependent HPV18 life cycle. *PLoS Pathogens*. 2018;14:e1006975.
- Morgan EL, Macdonald A. Autocrine STAT3 activation in HPV positive cervical cancer through a virus-driven Rac1-NFkappaB-IL-6 signalling axis. *PLoS Pathogens*. 2019;15:e1007835.
- Morgan EL, Macdonald A. JAK2 Inhibition Impairs Proliferation and Sensitises Cervical Cancer Cells to Cisplatin-Induced Cell Death. *Cancers (Basel)*. 2019;11:1934.
- Morgan EL, Macdonald A. Manipulation of JAK/STAT Signalling by High-Risk HPVs: Potential Therapeutic Targets for HPV-Associated Malignancies. *Viruses*. 2020;12:977.
- He C, Mao D, Hua G, Lv X, Chen X, Angeletti PC, et al. The Hippo/YAP pathway interacts with EGFR signaling and HPV oncoproteins to regulate cervical cancer progression. *EMBO Mol Med*. 2015;7:1426–49.
- Morgan EL, Patterson MR, Ryder EL, Lee SY, Wasson CW, Harper KL, et al. MicroRNA-18a targeting of the STK4/MST1 tumour suppressor is necessary for transformation in HPV positive cervical cancer. *PLoS Pathogens*. 2020;16:e1008624.
- Rose PG, Bundy BN, Watkins EB, Thigpen JT, Deppe G, Maiman MA, et al. Concurrent cisplatin-based radiotherapy and chemotherapy for locally advanced cervical cancer. *N Engl J Med*. 1999;340:1144–53.
- Ryu SY, Lee WM, Kim K, Park SI, Kim BJ, Kim MH, et al. Randomized clinical trial of weekly vs. triweekly cisplatin-based chemotherapy concurrent with radiotherapy in the treatment of locally advanced cervical cancer. *Int J Radiat Oncol Biol Phys*. 2011;81:e577–81.
- Zhu H, Luo H, Zhang W, Shen Z, Hu X, Zhu X. Molecular mechanisms of cisplatin resistance in cervical cancer. *Drug Des Devel Ther*. 2016;10:1885–95.
- Moore DH, Blessing JA, McQuellon RP, Thaler HT, Cella D, Benda J, et al. Phase III study of cisplatin with or without paclitaxel in stage IVB, recurrent, or persistent squamous cell carcinoma of the cervix: a gynecologic oncology group study. *J Clin Oncol*. 2004;22:3113–9.
- Santos R, Ursu O, Gaulton A, Bento AP, Donadi RS, Bologa CG, et al. A comprehensive map of molecular drug targets. *Nat Rev Drug Discov*. 2017;16:19–34.
- Lang F, Foller M, Lang KS, Lang PA, Ritter M, Gulbins E, et al. Ion channels in cell proliferation and apoptotic cell death. *J Membr Biol*. 2005;205:147–57.
- Blackiston DJ, McLaughlin KA, Levin M. Bioelectric controls of cell proliferation: ion channels, membrane voltage and the cell cycle. *Cell Cycle*. 2009;8:3527–36.
- Urrego D, Tomczak AP, Zahed F, Stuhmer W, Pardo LA. Potassium channels in cell cycle and cell proliferation. *Philos Trans R Soc Lond B Biol Sci*. 2014;369:20130094.
- Prevorskaya N, Skryma R, Shuba Y. Ion Channels in Cancer: Are Cancer Hallmarks Oncochannelopathies? *Physiol Rev*. 2018;98:559–621.
- Rosendo-Pineda MJ, Moreno CM, Vaca L. Role of ion channels during cell division. *Cell Calcium*. 2020;91:102258.
- Qian X, Li J, Ding J, Wang Z, Duan L, Hu G. Glibenclamide exerts an antitumor activity through reactive oxygen species-c-jun NH2-terminal kinase pathway in human gastric cancer cell line MGC-803. *Biochem Pharmacol*. 2008;76:1705–15.
- Nunez M, Medina V, Cricco G, Croci M, Cocca C, Rivera E, et al. Glibenclamide inhibits cell growth by inducing G0/G1 arrest in the human breast cancer cell line MDA-MB-231. *BMC Pharmacol Toxicol*. 2013;14:6.
- Ru Q, Tian X, Wu YX, Wu RH, Pi MS, Li CY. Voltage-gated and ATP-sensitive K<sup>+</sup> channels are associated with cell proliferation and tumorigenesis of human glioma. *Oncol Rep*. 2014;31:842–8.
- Yan B, Peng Z, Xing X, Du C. Glibenclamide induces apoptosis by activating reactive oxygen species dependent JNK pathway in hepatocellular carcinoma cells. *Biosci Rep*. 2017;37:BSR20170685.
- Vazquez-Sanchez AY, Hinojosa LM, Parraguirre-Martinez S, Gonzalez A, Morales F, Montalvo G, et al. Expression of KATP channels in human cervical cancer: Potential tools for diagnosis and therapy. *Oncol Lett*. 2018;15:6302–8.
- Seino S, Miki T. Physiological and pathophysiological roles of ATP-sensitive K<sup>+</sup> channels. *Prog Biophys Mol Biol*. 2003;81:133–76.
- Isomoto S, Kondo C, Yamada M, Matsumoto S, Higashiguchi O, Horio Y, et al. A novel sulfonylurea receptor forms with BIR (Kir6.2) a smooth muscle type ATP-sensitive K<sup>+</sup> channel. *J Biol Chem*. 1996;271:24321–4.
- Tinker A, Aziz Q, Li Y, Specterman M. ATP-Sensitive Potassium Channels and Their Physiological and Pathophysiological Roles. *Compr Physiol*. 2018;8:1463–511.
- Teisseyre A, Palko-Labuz A, Sroda-Pomianek K, Michalak K. Voltage-Gated Potassium Channel Kv1.3 as a Target in Therapy of Cancer. *Front Oncol*. 2019;9:933.
- Huang X, Jan LY. Targeting potassium channels in cancer. *J Cell Biol*. 2014;206:151–62.
- Hover S, Foster B, Barr JN, Mankouri J. Viral dependence on cellular ion channels - an emerging anti-viral target? *J General Virol*. 2017;98:345–51.
- DeFilippis RA, Goodwin EC, Wu L, DiMaio D. Endogenous human papillomavirus E6 and E7 proteins differentially regulate proliferation, senescence, and apoptosis in HeLa cervical carcinoma cells. *J Virol*. 2003;77:1551–63.
- Jabbar SF, Abrams L, Glick A, Lambert PF. Persistence of high-grade cervical dysplasia and cervical cancer requires the continuous expression of the human papillomavirus type 16 E7 oncogene. *Cancer Res*. 2009;69:4407–14.
- Jabbar SF, Park S, Schweizer J, Berard-Bergery M, Pitot HC, Lee D, et al. Cervical cancers require the continuous expression of the human papillomavirus type 16 E7 oncoprotein even in the presence of the viral E6 oncoprotein. *Cancer Res*. 2012;72:4008–16.
- Mikhailov MV, Mikhailova EA, Ashcroft SJ. Molecular structure of the glibenclamide binding site of the beta-cell K(ATP) channel. *FEBS Lett*. 2001;499:154–60.
- Brauner T, Hulser DF, Strasser RJ. Comparative measurements of membrane potentials with microelectrodes and voltage-sensitive dyes. *Biochim Biophys Acta*. 1984;771:208–16.
- Epps DE, Wolfe ML, Groppi V. Characterization of the steady-state and dynamic fluorescence properties of the potential-sensitive dye bis-(1,3-dibutylbarbituric

- acid)trimethine oxonol (Dibac4(3)) in model systems and cells. *Chem Phys Lipids*. 1994;69:137–50.
46. Wasson CW, Morgan EL, Muller M, Ross RL, Hartley M, Roberts S, et al. Human papillomavirus type 18 E5 oncogene supports cell cycle progression and impairs epithelial differentiation by modulating growth factor receptor signalling during the virus life cycle. *Oncotarget*. 2017;8:103581–600.
  47. Knight GL, Pugh AG, Yates E, Bell I, Wilson R, Moody CA, et al. A cyclin-binding motif in human papillomavirus type 18 (HPV18) E1<sup>E4</sup> is necessary for association with CDK-cyclin complexes and G2/M cell cycle arrest of keratinocytes, but is not required for differentiation-dependent viral genome amplification or L1 capsid protein expression. *Virology*. 2011;412:196–210.
  48. Jeon S, Lambert PF. Integration of human papillomavirus type 16 DNA into the human genome leads to increased stability of E6 and E7 mRNAs: implications for cervical carcinogenesis. *Proc Natl Acad Sci USA*. 1995;92:1654–8.
  49. Zhang W, Liu HT. MAPK signal pathways in the regulation of cell proliferation in mammalian cells. *Cell Res*. 2002;12:9–18.
  50. Huang L, Li B, Li W, Guo H, Zou F. ATP-sensitive potassium channels control glioma cells proliferation by regulating ERK activity. *Carcinogenesis*. 2009;30:737–44.
  51. Huang L, Li B, Tang S, Guo H, Li W, Huang X, et al. Mitochondrial KATP Channels Control Glioma Radioresistance by Regulating ROS-Induced ERK Activation. *Mol Neurobiol*. 2015;52:626–37.
  52. Shaulian E, Karin M. AP-1 as a regulator of cell life and death. *Nat Cell Biol*. 2002;4:E131–6.
  53. Macdonald A, Mazaleyrt S, McCormick C, Street A, Burgoyne NJ, Jackson RM, et al. Further studies on hepatitis C virus NS5A-SH3 domain interactions: identification of residues critical for binding and implications for viral RNA replication and modulation of cell signalling. *The J General Virol*. 2005;86:1035–44.
  54. Morgan EL, Scarth JA, Patterson MR, Wasson CW, Hemingway GC, Barba-Moreno D, et al. E6-mediated activation of JNK drives EGFR signalling to promote proliferation and viral oncoprotein expression in cervical cancer. *Cell Death Differ*. 2021;28:1669–87.
  55. Papavassiliou AG, Treier M, Bohmann D. Intramolecular signal transduction in c-Jun. *EMBO J*. 1995;14:2014–9.
  56. Treier M, Bohmann D, Mlodzik M. JUN cooperates with the ETS domain protein pointed to induce photoreceptor R7 fate in the *Drosophila* eye. *Cell*. 1995;83:753–60.
  57. Musti AM, Treier M, Bohmann D. Reduced ubiquitin-dependent degradation of c-Jun after phosphorylation by MAP kinases. *Science*. 1997;275:400–2.
  58. Wetherill LF, Holmes KK, Verow M, Muller M, Howell G, Harris M, et al. High-risk human papillomavirus E5 oncoprotein displays channel-forming activity sensitive to small-molecule inhibitors. *J Virol*. 2012;86:5341–51.
  59. Wetherill LF, Wasson CW, Swinscoe G, Kealy D, Foster R, Griffin S, et al. Alkyl-imino sugars inhibit the pro-oncogenic ion channel function of human papillomavirus (HPV) E5. *Antiviral Res*. 2018;158:113–21.
  60. Royle J, Dobson SJ, Muller M, Macdonald A. Emerging Roles of Viroproins Encoded by DNA Viruses: Novel Targets for Antivirals? *Viruses*. 2015;7:5375–87.
  61. Panou MM, Antoni M, Morgan EL, Loundras EA, Wasson CW, Welberry-Smith M, et al. Glibenclamide inhibits BK polyomavirus infection in kidney cells through CFTR blockade. *Antiviral Res*. 2020;178:104778.
  62. Carden H, Dallas ML, Hughes DJ, Lippitt JD, Mankouri J, Whitehouse A. Kv1.3 induced hyperpolarisation and Cav3.2-mediated calcium entry are required for efficient Kaposi's sarcoma-associated herpesvirus lytic replication. *bioRxiv*. 2021. <https://doi.org/10.1101/2021.09.10.459757>.
  63. Dobson SJ, Mankouri J, Whitesoe G. Identification of potassium and calcium channel inhibitors as modulators of polyomavirus endosomal trafficking. *Antiviral Res*. 2020;179:104819.
  64. Dubey RC, Mishra N, Gaur R. G protein-coupled and ATP-sensitive inwardly rectifying potassium ion channels are essential for HIV entry. *Sci Rep*. 2019;9:4113.
  65. Eleftherianos I, Won S, Chtarbanova S, Squiban B, Ocorr K, Bodmer R, et al. ATP-sensitive potassium channel (K(ATP))-dependent regulation of cardiotropic viral infections. *Proc Natl Acad Sci USA*. 2011;108:12024–9.
  66. Xu K, Sun G, Li M, Chen H, Zhang Z, Qian X, et al. Glibenclamide Targets Sulfonylurea Receptor 1 to Inhibit p70S6K Activity and Upregulate KLF4 Expression to Suppress Non-Small Cell Lung Carcinoma. *Mol Cancer Ther*. 2019;18:2085–96.
  67. Chen H, Zhao L, Meng Y, Qian X, Fan Y, Zhang Q, et al. Sulfonylurea receptor 1-expressing cancer cells induce cancer-associated fibroblasts to promote non-small cell lung cancer progression. *Cancer Lett*. 2022;536:215611.
  68. Chen M, Dong Y, Simard JM. Functional coupling between sulfonylurea receptor type 1 and a nonselective cation channel in reactive astrocytes from adult rat brain. *J Neurosci*. 2003;23:8568–77.
  69. Zerangue N, Schwappach B, Jan YN, Jan LY. A new ER trafficking signal regulates the subunit stoichiometry of plasma membrane K(ATP) channels. *Neuron*. 1999;22:537–48.
  70. Yuan H, Michelsen K, Schwappach B. 14-3-3 dimers probe the assembly status of multimeric membrane proteins. *Curr Biol*. 2003;13:638–46.
  71. Heusser K, Yuan H, Neagoe I, Tarasov AI, Ashcroft FM, Schwappach B. Scavenging of 14-3-3 proteins reveals their involvement in the cell-surface transport of ATP-sensitive K<sup>+</sup> channels. *J Cell Sci*. 2006;119:4353–63.
  72. Takahashi A, Yamaguchi H, Miyamoto H. Change in K<sup>+</sup> current of HeLa cells with progression of the cell cycle studied by patch-clamp technique. *Am J Physiol*. 1993;265:C328–36.
  73. Arcangeli A, Bianchi L, Becchetti A, Faravelli L, Coronello M, Mini E, et al. A novel inward-rectifying K<sup>+</sup> current with a cell-cycle dependence governs the resting potential of mammalian neuroblastoma cells. *J Physiol*. 1995;489:455–71.
  74. Pardo LA, Bruggemann A, Camacho J, Stuhmer W. Cell cycle-related changes in the conducting properties of r-eag K<sup>+</sup> channels. *J Cell Biol*. 1998;143:767–75.
  75. Ouadid-Ahidouch H, Roudbaraki M, Delcourt P, Ahidouch A, Joury N, Prevarskaya N. Functional and molecular identification of intermediate-conductance Ca(2+)-activated K(+) channels in breast cancer cells: association with cell cycle progression. *Am J Physiol Cell Physiol*. 2004;287:C125–34.
  76. Cripe TP, Alderborn A, Anderson RD, Parkkinen S, Bergman P, Haugen TH, et al. Transcriptional activation of the human papillomavirus-16 P97 promoter by an 88-nucleotide enhancer containing distinct cell-dependent and AP-1-responsive modules. *New Biol*. 1990;2:450–63.
  77. Butz K, Hoppe-Seyler F. Transcriptional control of human papillomavirus (HPV) oncogene expression: composition of the HPV type 18 upstream regulatory region. *J Virol*. 1993;67:6476–86.
  78. Kyo S, Klumpp DJ, Inoue M, Kanaya T, Laimins LA. Expression of AP1 during cellular differentiation determines human papillomavirus E6/E7 expression in stratified epithelial cells. *J General Virol*. 1997;78:401–11.
  79. Luna AJ, Sterk RT, Griego-Fisher AM, Chung JY, Berggren KL, Bondu V, et al. MEK/ERK signaling is a critical regulator of high-risk human papillomavirus oncogene expression revealing therapeutic targets for HPV-induced tumors. *PLoS Pathogens*. 2021;17:e1009216.
  80. Mankouri J, Taneja TK, Smith AJ, Ponnambalam S, Sivaprasadarao A. Kir6.2 mutations causing neonatal diabetes prevent endocytosis of ATP-sensitive potassium channels. *EMBO J*. 2006;25:4142–51.
  81. Morgan EL, Patterson MR, Barba-Moreno D, Scarth JA, Wilson A, Macdonald A. The deubiquitinase (DUB) USP13 promotes Mcl-1 stabilisation in cervical cancer. *Oncogene*. 2021;40:2112–29.
  82. Bristol ML, James CD, Wang X, Fontan CT, Morgan IM. Estrogen Attenuates the Growth of Human Papillomavirus-Positive Epithelial Cells. *mSphere*. 2020;5:e00049–20.
  83. Sundqvist A, Voytyuk O, Hamdi M, Popeijus HE, van der Burgt CB, Janssen J, et al. JNK-Dependent cJun Phosphorylation Mitigates TGFβ<sub>2</sub>- and EGF-Induced Pre-Malignant Breast Cancer Cell Invasion by Suppressing AP-1-Mediated Transcriptional Responses. *Cells*. 2019;8:1481.
  84. Jiang M, Milner J. Selective silencing of viral gene expression in HPV-positive human cervical carcinoma cells treated with siRNA, a primer of RNA interference. *Oncogene*. 2002;21:6041–8.
  85. Hall AH, Alexander KA. RNA interference of human papillomavirus type 18 E6 and E7 induces senescence in HeLa cells. *J Virol*. 2003;77:6066–9.
  86. Wilson R, Ryan GB, Knight GL, Laimins LA, Roberts S. The full-length E1E4 protein of human papillomavirus type 18 modulates differentiation-dependent viral DNA amplification and late gene expression. *Virology*. 2007;362:453–60.
  87. Livak KJ, Schmittgen TD. Analysis of relative gene expression data using real-time quantitative PCR and the 2(-Delta Delta C(T)) Method. *Methods*. 2001;25:402–8.
  88. Varghese F, Bukhari AB, Malhotra R, De A. IHC Profiler: an open source plugin for the quantitative evaluation and automated scoring of immunohistochemistry images of human tissue samples. *PLoS ONE*. 2014;9:e96801.
  89. Schneider CA, Rasband WS, Eliceiri KW. NIH Image to ImageJ: 25 years of image analysis. *Nat Methods*. 2012;9:671–5.
  90. den Boon JA, Pyeon D, Wang SS, Horswill M, Schiffman M, Sherman M, et al. Molecular transitions from papillomavirus infection to cervical precancer and cancer: Role of stromal estrogen receptor signaling. *Proc Natl Acad Sci USA*. 2015;112:E3255–64.

## ACKNOWLEDGEMENTS

We are grateful to Prof Felix Hoppe-Seyler (DKFZ), Dr Iain Morgan (VCU), Prof Eric Blair (University of Leeds), Dr Hans van Dam (LUMC) and Prof Greg Towers (UCL) for provision of reagents. We thank the Scottish HPV Investigators Network (SHINE), Prof Sheila Graham (University of Glasgow), Dr David Millan (University of Glasgow) and Prof Nick Coleman (University of Cambridge) for providing HPV positive patient samples.

## AUTHOR CONTRIBUTIONS

Conceptualisation (JAS, CWW, JM, ELM, AM); Formal analysis (JAS, CWW, MRP, HC, ELM); Funding acquisition (AW, AS, ELM, AM); Investigation (JAS, CWW, MRP, DE, HC, RC, ELM); Project administration (AW, AS, AM); Resources (DBM); Supervision (AW, AS, AM); Writing—original draft (JAS); Writing—review & editing (all authors).

## FUNDING

Work in the Macdonald lab is supported by Medical Research Council (MRC) funding (MR/K012665 and MR/S001697/1). JAS is funded by a Faculty of Biological Sciences, University of Leeds Scholarship. MRP is funded by a Biotechnology and Biological Sciences Research Council (BBSRC) studentship (BB/M011151/1). ELM was supported by the Wellcome Trust (1052221/Z/14/Z and 204825/Z/16/Z). HC was funded by a Rosetrees Trust PhD studentship awarded to AW (M662). AS is funded by CRUK (C50189/A29039). The funders had no role in study design, data collection and analysis, decision to publish, or preparation of the paper.

## COMPETING INTERESTS

The authors declare no competing interests.

## ADDITIONAL INFORMATION

**Supplementary information** The online version contains supplementary material available at <https://doi.org/10.1038/s41388-023-02772-w>.

**Correspondence** and requests for materials should be addressed to Ethan L. Morgan or Andrew Macdonald.

**Reprints and permission information** is available at <http://www.nature.com/reprints>

**Publisher's note** Springer Nature remains neutral with regard to jurisdictional claims in published maps and institutional affiliations.



**Open Access** This article is licensed under a Creative Commons Attribution 4.0 International License, which permits use, sharing, adaptation, distribution and reproduction in any medium or format, as long as you give appropriate credit to the original author(s) and the source, provide a link to the Creative Commons license, and indicate if changes were made. The images or other third party material in this article are included in the article's Creative Commons license, unless indicated otherwise in a credit line to the material. If material is not included in the article's Creative Commons license and your intended use is not permitted by statutory regulation or exceeds the permitted use, you will need to obtain permission directly from the copyright holder. To view a copy of this license, visit <http://creativecommons.org/licenses/by/4.0/>.

© The Author(s) 2023